Proteomic signatures for idiopathic cases of male infertility

Krmpotić, Klara

University of Zagreb
Faculty of Science
Department of Biology

Klara Krmpotić

Proteomic signatures for idiopathic cases of male infertility

Master thesis

Munich, 2021.

Sveučilište u Zagrebu
Prirodoslovno-matematički fakultet
Biološki odsjek

Klara Krmpotić

Proteomski obrasci idiopatskih slučajeva muške neplodnosti

Diplomski rad

München, 2021.

This master thesis was created in the Imhof group at the Biomedical Center Munich (BMC) of Ludwig Maximillian's University in Munich under the supervision of Professor Axel Imhof, co-supervision of postdoctoral fellow Shibo Lahiri, and Professor Dubravka Hranilović. The thesis was submitted for evaluation to the Department of Biology at the Faculty of Science, University of Zagreb to acquire the academic title of the Master of Molecular Biology.

Firstly, I would like to thank Prof. Axel Imhof for the opportunity to do a master thesis research in his group. I would also like to express my sincere gratitude to my mentor Shiboyoti Lahiri for sharing his mass spec expertise with me, numerous great advice and challenging me to do better. Big thanks to Dr. Ignasi Forne for his help with LC-MS improvements and measurements and Wasim Aftab for providing me with the ImShot software and answering all R and software related questions. Additional thanks to Dr. Andreas Thomae for teaching me how the Leica software works and for always being availabile and approachable. Furthermore, I am thankful to my co-mentor Prof. Dubravka Hranilović for all the advice and help with my thesis, and the knowledge passed on through the courses. Thank you all for investing your time and effort, it is appreciated.

I have been so fortunate to be able to work in the lab with such supporting and welcoming members. Special thanks to Anu for all late-night dinners, discussions and unwavering support whenever I needed it. You are a true friend and the best colleague person could wish for. Fredi, for all the laughter and joy you bring to the lab, your encouragement and kindness even in the most stressful of times.

And finally, a huge thanks to my family and friends. Thank you for your endless support, love and understanding. Iva and Kim, thank you for being there from start to finish, having you by my side made all the difference. Thank you for listening to all the voice messages and being in my corner - my supportive entourage. Happy to see where the road will lead us next. Marin, for being awesome and submitting my thesis. And for being the irreplaceable childhood and university friend. Hope our paths cross once again! Nikolina, for checking up on me all the time no matter how many times I forgot to answer your messages. Appreciate your care and love, know that it is reciprocated.

To my amazing non-uni friends, who are always there no matter how little we get to see each other, I love you. Andrea, Haller, Patrik, Marija and Evelin, my life is better with you in it.

To Ksenija, and Lea and Damir, my 'other' family. Thank you for always being there since I was a little 10-year-old child with animal stickers. For accepting me as a part of your own. You know how much you mean to me.

Thanks and love to my grandparents who called persistently in worry if the thesis will ever come to an end and for loving me unconditionally. To my parents and brother, who gave me the space I sometimes needed, but who were always in my corner. Love you.

Lastly, thanks to my boy, who was there every day, during good and bad, happiness and stress, joy and agitation, who shared a room with me and 'rarely' complained – Boris. I really appreciate the love and support you have shown me throughout this period. Hope to be that rock for you in the future.

BASIC DOCUMENTATION CARD

University of Zagreb
Faculty of Science
Department of Biology

Master Thesis

Proteomic signatures for idiopathic cases of male infertility

Klara Krmpotić

Rooseveltov trg 6, 10000 Zagreb, Croatia

Male infertility is a complex multifactorial disease whose underlying etiology remains unknown. Despite substantial efforts, 60–75% of the cases are classified as idiopathic, which makes them a subject of empirical and generalized treatments. This puts the impetus on a comprehensive understanding of the mechanisms of spermatogenesis and testis function thereby providing approaches to molecular diagnosis and targeted treatments. Azoospermia, characterized by the complete absence of sperm cells in seminal fluid, is one of the known conditions resulting in male infertility. To elucidate the complex molecular mechanisms causing male azoospermia, an approach combining high-resolution shotgun proteomics with imaging mass spectrometry (IMS) was carried out on testicular specimens from patients with mixed atrophy (MA) and spermatogenic arrest in spermatocyte 1 (SA). The obtained data showed dysregulation of spermatogenesis and emergence of hemostasis and pro-inflammatory processes in both testicular phenotypes. Furthermore, the IMS analysis revealed inter-patient and inter-tubular variability in the MA samples along with the region-specific dysregulation of basic cellular functions in both SA and MA samples. In conclusion this approach enabled to identify the molecular processes resulting in male infertility along with cell types and/or the tissue compartments responsible for it. It would potentially be instrumental in assessment of diseases and formulation of treatment strategies within tissues with complex and heterogeneous structure.

(88 pages, 21 figures, 2 tables, 128 references, original in: English)

Thesis is deposited in Central Biological Library.
Keywords: IMS, shotgun proteomics, azoospermia, idiopathic, mixed atrophy, spermatogenic arrest, testicular
Supervisor: Prof. Axel Imhof
Co-supervisor: Prof. Dubravka Hranilović

Reviewers:
Prof. Dubravka Hranilović
Assoc. Prof. Petra Peharec Štefanić
Asst. Prof. Romana Gračan
Asst. Prof. Sofia Ana Blažević (substitution)

Thesis accepted: 15th September 2021

TEMELJNA DOKUMENTACIJSKA KARTICA

Sveučilište u Zagrebu
Prirodoslovno-matematički fakultet
Biološki odsjek Diplomski rad

Proteomski obrasci idiopatskih slučajeva muške neplodnosti

Klara Krmpotić

Rooseveltov trg 6, 10000 Zagreb, Hrvatska

Muška neplodnost je složena multifaktorska bolest čija je etiologija i dalje nepoznata. Unatoč značajnim naporima, 60–75% slučajeva klasificirano je kao idiopatsko pa je i njihovo liječenje empirijsko i generalizirano. Zato postoji potreba za sveobuhvatnim razumijevanjem mehanizma spermatogeneze i funkcije testisa koje bi omogućilo nove pristupe molekularnoj dijagnostici i ciljanim tretmanima. Azoospermija, koju karakterizira potpuni nedostatak spolnih stanica u sjemenoj tekućini, jedno je od poznatih stanja koje rezultira muškom neplodnošću. Kako bi se razjasnili složeni molekularni mehanizmi koji uzrokuju mušku azoospermiju, provedeno je istraživanje, koje kombinira sposobnost "shotgun" proteomike visoke razlučivosti sa slikovnom spektrometrijom masa, na uzorcima testisa pacijenata s mješovitom atrofijom (MA) i spermatogenim zastojem u spermatocitu 1 (SA). Dobiveni podaci ukazuju na disregulaciju spermatogeneze i pojavu hemostaze i proupalnih procesa u oba fenotipa testisa. Nadalje, IMS analiza otkrila je varijabilnost među pacijentima i među sjemenim kanalićima u uzorcima MA, zajedno s regionalno specifičnom disregulacijom osnovnih staničnih funkcija u SA i MA uzorcima. Zaključno, ovaj pristup omogućio je identificiranje molekularnih procesa koji rezultiraju muškom neplodnošću zajedno sa, za to odgovornim, tipovima stanica i/ili odjeljcima tkiva. Ovaj pristup potencijalno bi mogao biti važan u procjeni bolesti i formuliranju strategija liječenja u tkivima sa složenom i heterogenom strukturom.

(88 stranica, 21 slika, 2 tablice, 128 literaturnih navoda, jezik izvornika: engleski)
Rad je pohranjen u Središnjoj biološkoj knjižnici
Ključne riječi: IMS, „shotgun" proteomika, azoospermija, idiopatsko, mješovita atrofija, spermatogeni zastoj, testis
Voditelj: Prof. dr. sc. Axel Imhof
Suvoditelj: Prof. dr. sc. Dubravka Hranilović

Ocjenitelji: Prof. dr. sc. Dubravka Hranilović
Izv. prof. dr. sc. Petra Peharec Štefanić
Doc. dr. sc. Romana Gračan
Doc. dr. sc. Sofia Ana Blažević (zamjena)
Rad prihvaćen: 15.09.2021.

Abbreviations

AUC – area under the curve

ACN – acetonitrile

AR – antigen retrieval

FFPE – formalin-fixed paraffin-embedded

FSH – follicle-stimulating hormone

H&E – hematoxylin and eosin

HP –heating under high pressure with differential power

IMS – imaging mass spectrometry

MALDI – matrix-assisted laser desorption/ionization

LC–MS – liquid chromatography–mass spectrometry

LH – luteinizing hormone

m – the molecular or atomic mass

NH_4HCO_3 – ammonium bicarbonate

NOA – non-obstructive azoospermia

OA – obstructive azoospermia

OI – overnight incubation

z – the electrostatic charge unit

Table of contents

1. Introduction

1.1. Idiopathic male infertility

Infertility presents a significant health concern that affects around 15% of couples of reproductive age worldwide amounting to 48.5 million couples (Griswold, 2016; Mascarenhas et al., 2012; Song et al., 2016). Although up to 50% of cases overall are solely due to male factor, male reproductive health has mostly remained poorly investigated to truly understand its magnitude and importance (Cassatella et al., 2013; Petok, 2015). Additionally, to this day, there is no accurate estimation of the global male infertility rate due to infrequent and inaccurate reporting, resulting mostly from cultural stigmas and lack of diagnosis of asymptomatic infertile men (Agarwal et al., 2015). In recent years, male infertility has gained very high momentum in the field of biomedical research owing to an alarming decline in sperm count and quality by almost 60% in less than 40 years. This resulted in increased global rates of male infertility (from 2.5% up to 12%) and has raised concern about male fertility in the future (Agarwal et al., 2015; Levine et al., 2017; Milewski et al., 2013).

1.1.1. Causes of male infertility

Multiple factors, including genetic, environmental and behavioral, are associated with male fertility (Cooke & Saunders, 2002; Nordkap et al., 2012). Among the above-mentioned factors, genetic etiology solely contributes to about 30% of all male infertility cases (Cooke & Saunders, 2002; Lilford et al., 1994). Abnormalities like sex chromosome aneuploidy, chromosome translocations and Y chromosome microdeletions are the most common genetic causes of impaired male fertility (Song et al., 2016). However, due to the highly complex genetic landscape responsible for male fertility, the underlying basis of most infertility cases remains unknown (Cooke & Saunders, 2002; Song et al., 2016).

To add a further level of complicacy, not only the genes but also the epigenetic factors play a significant role in the growing incidence of male fertility defects (Dada et al., 2012). The decreasing trend in sperm quality and overall impaired male reproductive function in the last few decades has been correlated with excess exposure to and high discharge of

environmental contaminants (heavy metals, food additives, plastics, pesticides) into the environment and food chain (Selvaraju et al., 2020). This can impair the male reproductive function through a variety of mechanisms, including altered epigenetic profiles. Recent studies have shown that exposure at both the developmental and adult stage could lead to a deterioration of testicular architecture and decreased sperm quality (Dada et al., 2012).

Male infertility contains a spectrum of phenotypes often with a complex etiology. Numerous anatomical and physiological features have been associated with infertility in men, but precise causative molecular mechanisms have remained elusive so far. In spite of the high frequency of occurrence, a substantial percentage of male infertility cases have no identifiable etiology and thus are classified as idiopathic that makes them a subject of empirical and generalized treatments (Bonanomi et al., 2002; De Kretser & Baker, 1999). Due to a lack of knowledge of the underlying cause and precise diagnosis, assisted reproductive technologies (ART) often are the only possibility that result in biological offspring (Fisher & Hammarberg, 2012; Stuppia et al., 2015). Currently, treatments for male infertility are limited and techniques like ART are used to circumvent rather than to treat a variety of male infertility issues (Cooke & Saunders, 2002). Consequently, this puts the impetus on a comprehensive understanding of the molecular basis of spermatogenesis and testis function that serves as a source of infertility.

1.1.2. Testicular structure, function and immunity

The testis is a very heterogeneous and intricate organ with a unique and highly organized anatomy that contains a great number of different cell types. It is histologically composed of two distinct regions: the exocrine part (seminiferous tubules) and an endocrine part (interstitial spaces). The entire process of sperm production, by which spermatogonial stem cells develop into highly specialized, motile spermatozoa, occurs within the seminiferous tubules of the testis (Figure 1) (Li et al., 2012). The seminiferous tubules are highly organized structures that contain two types of cells: somatic Sertoli cells and germ cells at different developmental stages, with the more mature cells lying closer to the central lumen. Sertoli cells form tight associations with germ cells undergoing progressive differentiation while providing them with structural and nutritional support and protection. Additionally,

interstitial (Leydig cells and various immune cells) and peritubular myoid cells that are present in the testicular interstitial spaces and the wall of the seminiferous tubules significantly contribute to the stem cell niche. Among them, Leydig cells are of crucial importance because of their ability to produce and secrete testosterone, which is critical for the maintenance of spermatogenesis and reproductive function in males (Cooke & Saunders, 2002). Besides Leydig cells, interstitium also contains components of the immune system, including blood and lymphatic vessels, as well as many types of immune cells such as macrophages, dendritic cells, mast cells, and T cells that are important for maintaining the special immunological environment of the testes (Li et al., 2012). The testis is a distinct immune privilege site where both allo- and auto-antigens are tolerated (Mellor & Munn, 2006). Since a large number of novel antigens are expressed in developing germ cells long after the establishment of immune tolerance, and could thus be recognized as "foreign" by the immune system, the maintenance of testicular immunoprivilege is of critical importance. Without it, immunogenic germ cells would evoke strong autoimmune responses resulting in their immune rejection (Li et al., 2012; Zhao et al., 2014). The testicular immunoprivilege is maintained by both systemic immune tolerance and active local immunosuppression. Multiple immunoregulatory mechanisms contribute to the immune privilege of the testis including: (1) the immunosuppressive properties of local testis-specific and immune cells; and (2) the special physical structure of the testis itself that involves the formation of blood-testis barrier (BTB) (Meinhardt & Hedger, 2011). The BTB is formed by various cellular junctions between neighboring Sertoli cells near the basal side of the seminiferous epithelium which is, thus, divided into the basal and adluminal compartments. This anatomical barrier also possesses physiological and immunological properties whose interaction creates a suitable microenvironment for spermatogenesis. It essentially prevents the passage of immune cells and factors from the circulation and interstitium to enter the inner part of the seminiferous tubules and be exposed to meiotic and haploid germ cells (Cheng & Mruk, 2012; Li et al., 2012). Therefore, if the BTB is functionally impaired, immunogenic germ cells within the adluminal compartments are no longer isolated from the immune components leading to an induction of chronic testicular inflammation (Naito et al., 2012).

Moreover, the testicular tissue can be infected by various pathogenic microorganisms via hematogenous dissemination from circulating blood and ascending genitourinary tracts. To elicit an appropriate and effective local immune response against invading pathogens, testicular cells have to overcome immune privilege (Zhao et al., 2014). This is achieved by generating an efficient antimicrobial innate immune defense. Nevertheless, disruption of the immune homeostasis by unrestrictive innate immune response may also lead to inflammation and ultimately result in impaired fertility (Li et al., 2012; Zhao et al., 2014). Testicular inflammation, caused by microbial infection or by noninfectious factors, is characterized by the infiltration of leukocytes into the testis and damage to the seminiferous tubules involving the shedding and apoptosis of sperm germ cells (Naito et al., 2012).

The exocrine function of the testes consists of the production of functional spermatozoa during the process called spermatogenesis. Since spermatozoa represent the vehicle by which male genetic information is passed from generation to generation, normal spermatogenesis is essential for species preservation and genetic variation (Oatley & Brinster, 2008). Spermatogenesis is a highly coordinated and intricate process, consisting of three distinct spatiotemporal phases. In the first, proliferative phase, spermatogonial stem cells (SSCs) undergo extensive mitotic division that results in both self-renewal and differentiation into primary spermatocytes that enter the second phase. Next, in the second meiotic phase, series of meiotic divisions and genetic recombination occur leading to the formation of haploid secondary spermatocytes and round spermatids. The third phase, termed spermiogenesis, involves the morphological transformation of round spermatids into mature spermatozoa (Griswold, 2016; Park & Pang, 2021). These phases leading to successful spermatogenesis involve complex molecular pathways that require a tightly coordinated activity of more than 2000 testis-specific genes (Hochstenbach & Hackstein, 2000). This makes the process highly vulnerable to the accumulation of errors that can easily result in impaired spermatogenesis (Song et al., 2016). However, the combined effect of many genes rather than defects in a single one is more likely to cause infertility (Cooke & Saunders, 2002; Song et al., 2016).

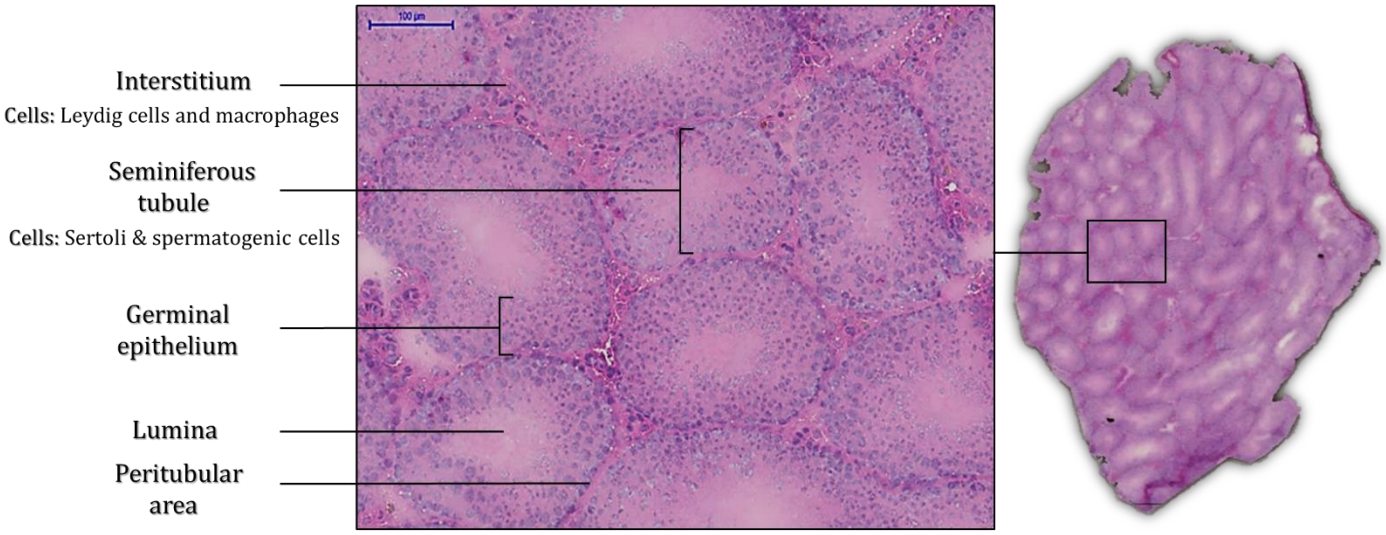

Figure 1. Representative testicular cross-section with defined main morphological compartments. Each testis consists of seminiferous tubules, which are surrounded by the peritubular area and embedded in the relatively sparse interstitial tissue. The interstitium contains two notable cell populations, Leydig and immune cells, while seminiferous tubules consist of a germinal epithelium surrounding the central lumen that contains spermatogenic and Sertoli cells. The peritubular area that separates these two compartments consists of peritubular myoid cells. The tissue was stained with hematoxylin and eosin; the black box shows the region in greater detail. Scale bar - 100 µm.

1.1.3. Research on male infertility

Despite the great progress made in the field of male reproduction since the beginning of the 20th century, approximately 50% of the cases of infertility are caused by idiopathic disturbance of spermatogenesis (Singh & Singh, 2017). Poor understanding of the etiology of those cases makes them a subject of empirical and generalized treatments. Furthermore, there is no standardized drug available for treating idiopathic infertility (Cooke & Saunders, 2002; Singh & Singh, 2017). Additionally, it is often the case that patients have no history of diseases affecting fertility and show normal findings of physical examinations and genetic, biochemical and endocrine laboratory testings (Bracke et al., 2018). As a consequence, andrology laboratories mostly rely on patient's semen analysis that in about 70% of cases reveals abnormal semen parameters and is, thus, used for diagnosing male infertility (Bracke et al., 2018; Lenzi, 1995; Panner Selvam & Agarwal, 2017). A high-quality semen analysis is a

reliable measure of overall male fertility serving as an indicator of fertilization success and relative reproductive fitness (Xiao & Xia, 2016). It is inexpensive, easy to perform and provides valuable information that is generally used for treatment planning (Cummins & Jequier, 1994). It mainly relies on the measurement of sperm concentration, motility and morphology (Poongothai et al., 2009).

There are several phenotypic varieties of semen anomalies, ranging from azoospermia (i.e. absence of spermatozoa in semen), oligozoospermia (very low sperm count in the semen) to astheno- (abnormal sperm motility) and teratozoospermia (abnormal sperm morphology), out of which one or more are regularly found in almost 90% of infertile males (Krausz & Riera-Escamilla, 2018b). Out of those, azoospermia and oligospermia represent quantitative defects with reduced sperm count, while astheno- and teratozoospermia represent qualitative defects of sperm morphology or function (Poongothai et al., 2009). Since azoospermia represents a severe cause of male infertility with only 20% of currently known genetic causes and quite limited treatment options, it has received considerable research attention in recent years (Aziz, 2013). It is defined as a condition with the complete absence of sperm cells in the ejaculate. There are three main etiological categories of azoospermia: (1) pretesticular azoospermia that implies endocrine abnormalities and hypothalamic-pituitary failure; (2) testicular or non-obstructive azoospermia (NOA) that involves abnormal sperm production and intrinsic disorders in the testis; and (3) post-testicular or obstructive azoospermia (OA), that implies obstruction of the ductal system of the male reproductive tract (Cocuzza et al., 2013). In the case of obstructive, post-testicular azoospermia, the spermatogenic process remains unaffected and fully functional including normal levels of luteinizing hormone (LH) and follicle-stimulating hormone (FSH) and normal size testes (Hirsh, 2003; Jarvi et al., 2010). On the other hand, NOA can be phenotypically classified into at least three distinct subtypes of idiopathic spermatogenic disturbances, according to histopathology findings: (1) Sertoli-cell-mixed syndrome; (2) spermatogenic arrest (SA) at different stages of germ cell maturation; and (3) hypospermatogenesis (Cioppi et al., 2021). Additionally, it accounts for approximately 75% of the instance of male infertility (Krausz & Riera-Escamilla, 2018a). Sertoli-cell-mixed syndrome or otherwise known as mixed atrophy (MA) is observed in 25% of the testicular

biopsies from infertile men. It is characterized as a lesion with synchronous occurrence of both seminiferous tubules containing germ cells and tubules containing only Sertoli cells in variable proportions. These variable degrees of spermatogenic impairment can be observed in only few seminiferous tubules or can show distribution throughout the testicular biopsy specimen (Nistal et al., 2007). This common appearance of a heterogeneous phenotype throughout the testis presents a valuable research model in which any methodological reasons for possible unequal preparations and tissue handling are ruled out since both tubules with normal and impaired spermatogenesis can be found side by side (Maymon et al., 2002). On the other hand, maturation or spermatogenic arrest is a complex process of interruption of germ cell differentiation at the level of a specific cell type including spermatogonia, spermatocyte, and spermatid level. In contrast, hypospermatogenesis is defined as a decrease in the number of all germ cells in similar proportions while all the stages of spermatogenesis are present (Halder et al., 2015; Martin-du Pan & Campana, 1993). Despite extensive efforts, the underlying molecular etiology of non-obstructive azoospermia is in most cases still unknown and reflects our poor understanding of the mechanism governing spermatogenesis. In addition, various etiologies have similar histological phenotypes, which highlights the need for techniques that allow a much deeper understanding of the molecular and genetic pathways involved in the phenotype (Cooke & Saunders, 2002).

In order to explore underlying etiopathology, different genetic approaches including large-scale genomic studies have been applied (Krausz & Riera-Escamilla, 2018a). However, these methods do not provide crucial information on the post-transcriptional control of gene expression, global changes in protein constellation and protein modifications. Out of 15,000 transcripts present in a germ cell, only a small subset encodes for proteins involved in cell-type-specific functions. Therefore, the emergence of proteomics techniques that provide deep coverage of the cellular proteome turned up being crucial for a comprehensive assessment of cellular activities. By studying the global pattern of protein content and activity in response to disease, modern proteomics research is poised to help in the understanding of the pathways and proteins that are involved in infertility conditions (Jockusch et al., 2014). Therefore, testis and sperm proteomics serves as a promising tool in the identification of new

drug targets and the development of potential diagnostic and therapeutic biomarkers for the management of male infertility (Panner Selvam & Agarwal, 2017).

However, up to this point, most proteomic studies have been concentrated on researching sperm or seminal plasma although the testis represents the primary organ in generating abnormalities that lead to arrest and eventually impaired reproductive function. Nevertheless, due to the invasive tissue sampling approach, as well as testicular heterogeneity, the research of testis has been particularly challenging (Krausz & Riera-Escamilla, 2018). Presently, there are only a few studies on proteomic analyses of the testicular tissue. However, they bear the disadvantage of low protein identification and the lack of spatiotemporal information. Hence, the precise causative molecular mechanisms that underlie a specific individual's infertility remained elusive and not fully understood (Cooke & Saunders, 2002; Liu et al., 2013; Macleod & Varmuza, 2013).

1.2. FFPE tissues

Formalin-fixed paraffin-embedded (FFPE) tissue biospecimens are frequently used for preserving patient tissues as they are viable over long periods at ambient temperatures without concern for degradation or decay. This cost-effective method allows archiving of a vast numbers of FFPE blocks (Greytak et al., 2015; Kokkat et al., 2013; O'Rourke & Padula, 2016). Therefore, since 1893 formalin fixation technique has been, and is still, the standard preservation process in clinical pathology (Giusti et al., 2019) and has served as a source of patient samples of various diseases (Giusti et al., 2019; Giusti & Lucacchini, 2013; Sy & Ang, 2019). These worldwide archives are an indispensable resource of clinical information that can be used for extensive retrospective studies allowing research of disease progression over the course of time (Giusti & Lucacchini, 2013). Additionally, this standard fixation method allows storing of tissue samples for an extended duration by effectively preserving the tissue morphology, cell structures and proteins. While fixation with formaldehyde, commonly known as formalin, halts cell metabolism and preserves the structural integrity within the tissue, embedding in paraffin wax block reduces the oxidation rates, seals the tissue and makes the tissue sectioning easier (Maraschin et al., 2017).

Although FFPE tissues have been traditionally used in histopathological and immunohistochemical studies, in the last decade the utilization of FFPE tissues for proteomic analysis has raised a great research interest due to easy accessibility and the potential wealth of information that FFPE archives hold (Giusti et al., 2019; Giusti & Lucacchini, 2013; O'Rourke & Padula, 2016). The research has been mostly focused on the identification of potential protein biomarkers, associated with various disorders, with predictive and prognostic value (Giusti et al., 2019; Giusti & Lucacchini, 2013). However, the main challenge in working with FFPE tissues is overcoming the effects of chemical protein modifications generated during formalin fixation that hinder the extraction of proteins. Formaldehyde reacts with amino groups of proteins through a multi-step process causing the formation of stable and extensive intra- and intermolecular crosslinks such as methylol adducts, Schiff's bases and stable methylene bridges. The bridge makes it challenging to ionize proteins, and study is therefore difficult when using FFPE for IMS. Additionally, FFPE process can disrupt

or remove proteins from the tissue, making protein analysis highly demanding (O'Rourke & Padula, 2016; Tanca et al., 2012). Another important issue in FFPE proteome research is the lack of a standardized protocol for reversing formaldehyde-induced modifications. Therefore, reliable and robust sample preparation protocols are needed in order to increase the accessibility of proteins from FFPE sections and in that way achieve a more complete proteomic profile (Giusti et al., 2019; O'Rourke & Padula, 2016).

The development of various strategies for the recovery and extraction of full-length proteins or peptides has allowed proteomic investigation of FFPE archival tissues. The antigen retrieval (AR) method, was developed by Shi and coworkers in 1991 and has led to the restoration of the antigen immunoreactivity and elevated protein extraction yield (Shi et al., 1991; Tanca et al., 2012) from FFPE tissues. Briefly, the method includes boiling the tissue sections in the aqueous extraction buffer of pH 7.0 or 9.0 that leads to reversal of formaldehyde crosslinked network and ultimately to the restoration of antigenic properties. A second approach includes direct proteolytic digestion of the fixed tissue, followed by shotgun or targeted proteomic analysis. Hence, the first strategy leads to the delivery of full-length protein extract, while the second approach generates a peptide mixture directly from the tissue sample, and may thus not be applicable for downstream techniques analyzing full-length proteins. In addition, some protocols include combinations of the two approaches (Tanca et al., 2012). In summary, once the protein extraction protocols have been adequately optimized, the proteomic analysis of tissues can follow. In this way, utilization of these new powerful proteomic techniques that have recently evolved offers new opportunities in biomedical research (Steiner et al., 2014).

1.3. Mass spectrometry - based proteomics

Over the last two decades, new strategies of proteomic analysis have appeared, out of which mass spectrometry has emerged as the most valuable and indispensable tool for large-scale protein analysis. This powerful analytical technique has great potential for biological and clinical research due to its ability to perform unbiased and in-depth biomolecular analysis of any type of tissue (Coscia et al., 2020; Longuespée et al., 2014; Zhang et al., 2013). In recent years, there has been a rapid technological advancement of MS instrumentations in the sensitivity, resolution, mass accuracy and scan rate (Zhang et al., 2013). This development enabled effective and accurate detection, identification, quantification and characterization of the proteins in a biological sample or system (Angel et al., 2012).

1.3.1. Shotgun proteomics

Bottom-up or shotgun proteomics is a high throughput technique for the measurement of protein abundances through the analysis of complex peptide mixtures. It is the most common MS-based method for protein identification (Yates III, 1998). In a bottom-up proteomics experiment, a mixture of proteins is isolated and enzymatically fragmented into peptides. The resulting peptide mixture is then fractionated using chromatography, ionized and subjected to MS and tandem MS (MS/MS) analysis (Zhang et al., 2013). In tandem MS measurement, peptides are fragmented within the mass analyzer in order to comprehend the amino acid composition of the corresponding peptide from mass to charge ratio (m/z) of the fragmented ions (Mittal, 2015). For the identification of proteins, data derived from the peptide fragmentation is searched against a theoretical peptide database that is followed by assigning peptide sequences to proteins (van Vliet, 2014; Zhang et al., 2013).

Shotgun proteomics is a powerful technique that combines the resolving power of liquid chromatography (based on peptide size and physicochemical properties) with the detection sensitivity and reliability of mass spectrometry (van Vliet, 2014). One of the main advantages of liquid chromatography-mass spectrometry (LC-MS) lies in its untargeted or label-free approach which makes the sample analysis unbiased and leads to the identification of several hundred to thousand proteins (Steiner et al., 2014). However, in the pathological analysis of

complex and highly heterogeneous tissues with many functional compartments such as the testis, it is of crucial importance not only to identify, but also to obtain the spatial distribution of the proteins present within the tissue. Unfortunately, the protein extraction/purification step in LC-MS requires tissue homogenization, which causes the complete loss of the spatial information. In order to acquire this information, which is essential for accurate understanding and translation of spatially resolved molecular information to tissue morphology, LC-MS is coupled with its complementary technique, imaging mass spectrometry (IMS) (Fujimura & Miura, 2014; Irie et al., 2014; Lahiri et al., 2021).

1.3.2. Imaging mass spectrometry

In contrast to shotgun proteomics, IMS is performed directly on intact tissue sections. Therefore, researchers can gain knowledge of the regional distribution of the biomolecules within their biological niche (Irie et al., 2014; Steiner et al., 2014).

Among the several imaging mass spectrometry ionization techniques, MALDI has developed as the leading one in the development of biological and clinical applications and is thus one of the most commonly used and described (Aichler & Walch, 2015). Besides preserving spatiotemporal information, another great advantage of this method is the accessibility of analytes ranging from proteins and peptides to metabolites and other small molecules that were not accessible before at this massive scale, even with classical histological strategies. Additionally, this state-of-the-art method is label-free and provides simultaneous mapping and analysis of hundreds of compounds of various natures in the very same tissue section (Aichler & Walch, 2015; Longuespée et al., 2014).

The matrix-assisted laser desorption/ionization (MALDI) IMS was introduced in the 1980s and since then immense improvements in the mass range, spatial and spectral resolution, analysis speed and data processing have been made (Longuespée et al., 2014). Therefore, due to its technological advancements and the broad range of features, the MALDI imaging technique was explored early on in biomarker discovery and as a clinical diagnostic tool in many ranging fields, from pathology to pharmacology (El Ayed et al., 2010; Longuespée et al., 2014).

In order to perform MALDI IMS analysis, a defined workflow must be strictly followed. The principal workflow of a MALDI imaging experiment consists of a sample preparation resulting in matrix application followed by the analysis in a MALDI mass spectrometer. Sample preparation for MALDI IMS is the most important aspect of the workflow, and thus must be carefully standardized and executed in order to achieve optimal results. It comprises of specimen collection and preservation, tissue embedding, sectioning, washing, and matrix application. The matrix co-crystallizes the analyte molecules from the tissue that is eventually detected by a mass spectrometer. In order to extract molecules, the laser shoots the matrix crystals at each x, y position of the virtual raster pattern (Figure 2). The matrix absorbs the laser energy causing desorption and ionization of analyte molecules. For each measuring spot, a mass spectrum is generated, reporting the intensities of mass-to-charge (m/z) ratios that relate to specific molecular species. Solvents are then used to remove the matrix from the section and it is routinely stained with hematoxylin and eosin (H&E) (Aichler & Walch, 2015).

However, when using FFPE tissues additional protocol optimization steps have to be implemented (Figure 2). Before matrix treatment, paraffin has to be removed with multiple washing steps after which the AR step has to be performed along with *in situ* enzymatic digestion (Gemoll et al., 2011). The protein identity of the measured *m/z* values can be assigned using mass matching to the calculated *m/z* values of the enzymatically cleaved peptides identified by LC–MS/MS with high resolution and high mass accuracy (Giusti & Lucacchini, 2013).

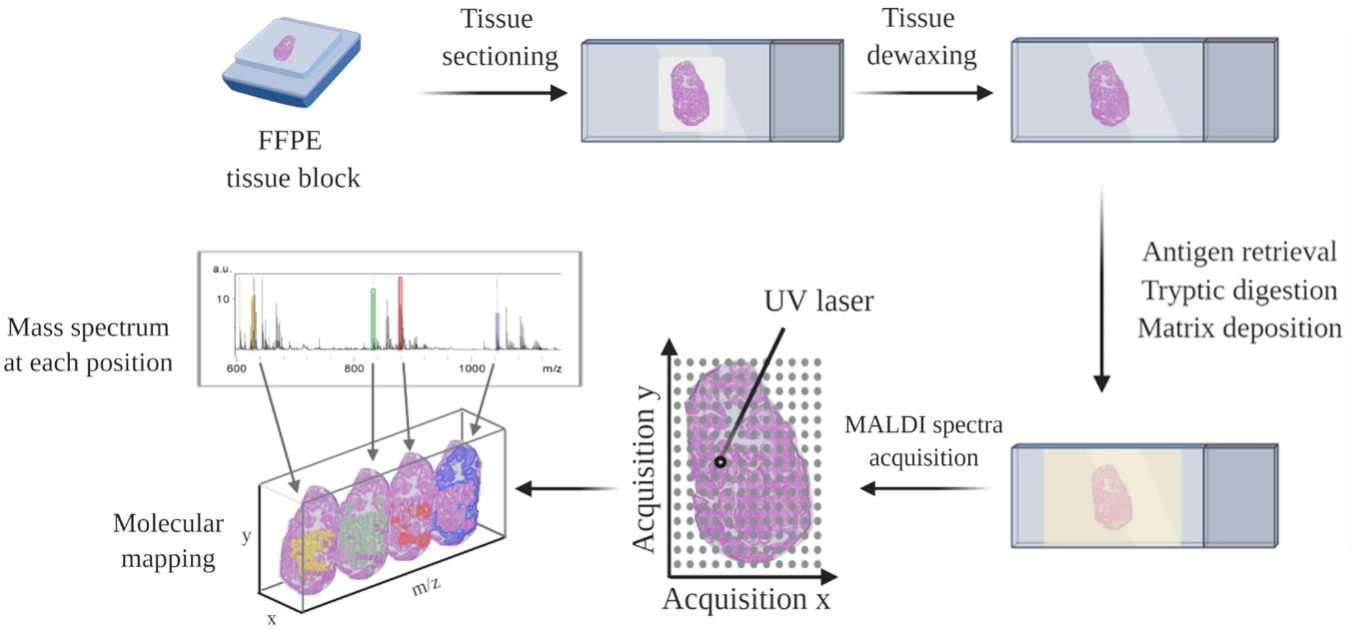

Figure 2. Schematic outline of a workflow for a MALDI IMS experiment using FFPE tissue samples. Sample treatment steps include tissue sectioning, mounting the sample on a target and deparaffinization, followed by additional steps required when using FFPE tissues such as antigen retrieval step, tryptic digestion and *in situ* incubation step. Afterward, tissue is coated with matrix and MS analysis starts. Mass spectra are generated in an ordered array at each x, y coordinate. Ion (*m/z* value) densities of various molecules can be spatially displayed with their relative intensity in the tissue section. Tissue – representative sample of human testis tissue (created with Biorender.com free version)

1.4. Aim of the study

Male reproductive health has been largely neglected and heavily stigmatized resulting in inadequate and outdated diagnostic methods that have remained mostly unchanged for the past 50 years (Ravitsky & Kimmins, 2019). In addition, male infertility is a multifactorial and complex disease, whose underlying molecular mechanisms remain unknown. As a result, most of the male infertility cases have been classified as idiopathic (Bracke et al., 2018). In order to develop novel approaches for molecular diagnosis and targeted treatments, a profound knowledge of the complex process of spermatogenesis and testis function is required.

Moreover, the samples for this study were acquired in the form of the FFPE tissues. Here, the formalin fixation step of this preservation technique generated crosslinking-based modifications that led to insufficient proteomic coverage.

Therefore, the aim of the study is to:

a) develop and optimize a comprehensive sample preparation protocol for the MALDI IMS analysis that will increase the accessibility of proteins while maintaining tissue integrity and preventing analyte delocalization and loss
b) make the comparative analysis of proteomic profiles of the testicular proteins expressed in healthy individuals and individuals with different types of spermatogenic impairments (MA and SA)
c) correlate this differential expression with morphological tissue features that will help in investigating and understanding which molecular processes are prominent in specific tissue compartments that will provide an in-depth understanding of precise molecular pathways and interactions involved in idiopathic cases of male infertility

In order to achieve this objective, a deep shotgun proteomic study of patient testes samples is performed to identify peptides present in each tissue specimen. Next, the acquired proteomic data is coupled with *in situ* spatial distribution information obtained with the MALDI IMS technique.

2. Materials and methods

2.1. Clinicopathological data and sample collection

Human testis tissues were obtained from patients who were undergoing pathological evaluation. Biopsies were performed by Dr. Frank-Michael Köhn at the andrology clinic "Andrologicum München". Following the biopsy, testis tissue was immediately fixed in formalin solution, embedded in paraffin and stored under standard conditions. Afterward, tissue samples were pathologically evaluated and categorized, based on the morphological criteria. Lastly, the tissue of testes with PS, MA and SA were provided by a collaborating partner Prof. Dr. Med. Artur Mayerhofer (Department for Cell Biology, Biomedical Center, LMU Munich, Medical Faculty) and were used in this study.

The study has been reviewed and approved by the Ethical Review Board due to the nature of the human subject involvement and the invasiveness of the sample collection. Furthermore, informed consent was obtained from patients whose testicular samples were used in this study.

Tissue samples were obtained from the testes of two patients with MA aged 52 and 53 years (MA1 and MA2) and one patient with SA aged 41 years (SA1). Two testicular biopsy samples were obtained from MA1 patient (MA1a and MA1b) and SA1 patient (SA1a and SA1b). Tissue specimens collected from one healthy fertile donor with preserved spermatogenesis (PS), aged 36 years (PS1), was used as control. Patients did not suffer from any diseases that obviously could cause impaired male reproductive health. Additional clinical information for each group is summarized in Table 1.

Tissue samples of mouse testis that were used for the protocol optimization purposes were obtained using the same tissue preservation method as the clinical samples.

Table 1. Summary of patient information. The table contains information regarding required testicle biopsy samples including number, patient age, FSH levels, medical histories and disease classification. FSH - follicle-stimulating hormone; PS1 – testicular biopsy derived from fertile donor with preserved spermatogenesis; MA1a – first testicular biopsy derived from first patient with mixed atrophy; MA1b – second testicular biopsy derived from first patient with mixed atrophy; MA2 – testicular biopsy derived from second patient with mixed atrophy; SA1a – first testicular biopsy derived from patient with spermatogenic arrest; SA1b - second testicular biopsy derived from patient with spermatogenic arrest

Histological classification	Patient number	Testicular biopsy	Patient age	FSH level (mIU/ml)	Medical condition	Clinical cassification
Preserved spermatogenesis	1	PS1	36	<10	azoospermia, epididymitis	OA
Mixed atrophy	2	MA1a & MA1b	52	23.9	azoospermia	NOA
		MA2	53	12.2	azoospermia	NOA
Spermatogenic arrest	1	SA1a & SA1b	41	14.7	azoospermia	NOA

2.2. Tissue sectioning and float mounting

FFPE testis tissue blocks from mouse and human subjects were sectioned into 12 and 4 µm thick sections using a microtome (Thermo) for LC-MS and MALDI IMS analysis, respectively. The LC-MS replicates were collected in protein low-bind Eppendorf tubes and stored at room temperature until further sample preparation and analysis.

Tissue sections of 4 µm, used for MALDI imaging, were float-mounted from a 47°C to 50°C water bath onto conductive indium-tin-oxide (ITO) coated glass slides (Bruker). Two tissue sections were mounted on each ITO coated glass slide. Beforehand, ITO slides were pretreated with poly-L-lysine (1:1 in water with 0.1% NP40) using a FelxiStrip spatula (Heinz Herenz) to improve tissue adhesion and to avoid the detachment of tissues from targets. Next, tissue sections were placed in an incubator at 60°C for one hour to allow them to dry and adhere to the slide. After incubation, the slides were stored at room temperature until further usage.

2.3. MALDI – imaging mass spectrometry

2.3.1. Sample preparation

2.3.1.1. Washing

Tissue slides were sequentially washed using two changes of xylene (three minutes each), following with a graded series of ethanol: two changes of 100% ethanol (one minute each), 95% ethanol (one minute), 70% ethanol (one minute) and two changes of Mili-Q purified water (three minutes each). Next, tissue sections were placed in a vacuum desiccator until they were completely dried.

2.3.1.2. Antigen retrieval method

In this study, two heat-induced epitope retrieval methods were tested:

a) Overnight incubation (OI): water bath
b) Heating under high pressure with differential power (HP): microwave pressure cooker

In both methods, the AR was performed using 10 mM Tris buffer, pH 9. In the case of O/N incubation, tissue sections were placed in a glass jar containing the buffer and sealed with parafilm. Next, tissue sections were incubated at 60-65°C using water bath Emmi-H40 (EMAG AG, Mörfelden-Walldorf, Germany) for 15-18h. Following antigen retrieval, the slide container was removed and left to cool at room temperature for 20 min (Judd et al., 2019).

In the second tested protocol, AR was performed using a pressure-regulated chamber placed inside of the scientific microwave. The tissue slides were placed in the non-sealed microwaveable vessel (with slide rack) containing 250 ml of 10 mM Tris buffer, pH 9. Next, the vessel was placed inside the pressure cooker (Microwave Tender Cooker®, Cat. No. 62104) filled with 600 ml of distilled water and centered inside the microwave. Slides were heated for about 15 min on high power (800W) until the cooker was fully pressurized. The solution was allowed to simmer for an additional 10 min at reduced microwave power level (400W). Afterward, the pressure cooker was removed from the microwave oven and opened allowing the slides to cool down for 20 minutes inside the cooker before the further cooling procedure (BioGenex, 2020).

The following steps were the same in both protocols: for further cooling, the buffer was exchanged by replacing half of the solution four times with Mili-Q water and then the whole solution with Mili-Q water. Subsequently, the tissue slides were vacuum dried and stored at RT before scanning and trypsin-spraying (Promega) (Judd et al., 2019).

2.3.1.3. On-tissue digestion

For optimization, two trypsin solutions were compared in order to determine which one ensures the optimal peptide yield while maintaining spatial fidelity:

a) 74 µg/mL of trypsin dissolved in 100 mM NH_4HCO_3 and 9% ACN (Judd et al., 2019)
b) 25 µg/mL of trypsin dissolved in 20 mM NH_4HCO_3 and 0.01% glycerol (Sigma) (Ly et al., 2019)

The solutions were applied using the syringe spray system of TM Sprayer (HTX Imaging, HTX Technologies, LLC). Same sprayer parameters were used for the deposition of both trypsin solutions. The nozzle temperature was set to 30 °C and was positioned 40 mm from the surface of the slide. Nitrogen was used as a carrier gas at 9.5 psi. Trypsin was delivered from the syringe to the sprayer at a flow rate of 8 µL/min. A total of 8 passes were completed at a rate of 750 mm/min in a criss-cross pattern, with 2 mm track spacing and no drying time (Judd et al., 2019).

Following trypsin deposition, the tissue sections had to be incubated in a humid digestion chamber. Two main digestion conditions parameters are the tissue hydration method and digestion time. To ensure an optimal trypsin activity, a solution of ammonium bicarbonate was used to create a humid atmosphere of approximately pH 7.4 (Wenke et al., 2015). The digestion chamber was prepared using a 92 x 16 mm plastic Petri dish with a 5 x 5 cm tissue square placed in the bottom of the dish, previously soaked with 120 µL of 100 mM ammonium bicarbonate in order to maintain the stable humidity. A single glass slide was placed inside each Petri dish and sealed with parafilm. The tissue sections were then incubated for the next 2.5 h using Mini Incubator (Labnet International) to allow sufficient time for the digestion reaction to occur (Judd et al., 2019).

However, two tissue hydration temperatures have been compared:

a) 37 °C (Judd et al., 2019)
b) 50 °C (Commercial, HTX)

2.3.1.4. Matrix deposition

The matrix deposition step was done according to the protocol for matrix application previously tested by Judd et al (2019). Based on their protocol, the slides were sprayed with purified alpha-cyano-4-hydroxycinnamic acid (CHCA) (Bruker) at a concentration of 5 mg/mL in 90% acetonitrile and 0.1% trifluoroacetic acid (TFA) using a robotic sprayer (HTX TM Sprayer model M3). To dissolve CHCA solution, sonication in the duration of 3 min was required.

Matrix was sprayed on tissue sections for a total of 8 passes at a nozzle velocity of 700 mm/min in a criss-cross pattern, with 2 mm track spacing and no drying time. 90% ACN was used as a pushing solvent at a flow rate of 0.1 mL/min. The nozzle of the HTX TM Sprayer was aligned 40 mm from the surface of the slide and the nitrogen carrier gas was set to 10 psi.

The parameter that was further optimized was the matrix deposition temperature, where two temperatures were thoroughly tested and compared between two tissue sections on the same slide:

a) 60 °C
b) 70 °C

Following matrix deposition, Peptide Calibration Standard II (Bruker) was mixed with the prepared matrix (1:2) and spotted on multiple positions on the slide before proceeding to the IMS measurement.

2.3.2. Imaging mass spectrometry measurement

MALDI imaging data was acquired using a rapifleX MALDI Tissuetyper MALDI-TOF/TOF mass spectrometer (Bruker) equipped with a SmartBeam 3D laser (355 mm). Data from the tissue samples were acquired at 20 μm spatial resolution in a positive ion reflector mode using a mass range of 600-3200 Da and a pulsed ion extraction of 160 ns. Spectra were accumulated from 500 laser shots per pixel at 10 kHz frequency with a sampling rate of 1.25 GS/s and baseline subtraction performed during acquisition. The "Detector check" function was conducted regularly before each measurement in order to adjust this variable setting at appropriate voltages. For every measurement, the instrument was externally calibrated using previously applied peptide calibrant spots. Additionally, the laser power was adjusted according to on-tissue test shots to reach the optimal ionization threshold intensity of 1×10^4 arbitrary units. Besides the measurement of the tissue regions, two non-tissue regions were also included in order to acquire the background spectra.

2.3.3. Histological staining and co-registration of the stained tissues

Following IMS measurement, the CHCA matrix was removed by washing the slides in 70% ethanol and stained with H&E. H&E staining consisted of the following steps: immersing the slides in distilled water for 3 minutes, hematoxylin for 2 min, rinsing the slides under tap water for 5 min and immersing in eosin (1g/L) solution for 2 min. Subsequent dehydration of the tissues included immersing the slides four times in 70%, 90% and 100% ethanol followed by 3 min immersion in isopropanol. Clearing the slides was done by rinsing the slides in xylol I and II for 5 min. Each slide was then coverslipped using standard type histological cover slips (24 x 60 × 0.16 mm) and mounted on to the tissue using a thin layer of Pertex mounting medium (VWR). Finally, each slide was let to dry for a period of 24 hours.

In order to obtain the high-resolution images of the stained sections, the samples were scanned using Leica Las X widefield microscope under transmitted light (Leica Microsystems). Images were acquired with 10× objective magnification in TileScan mode and subsequently smoothly merged. Afterward, the H&E images were directly co-registered to

the respective MALDI IMS measurement data images for histological correlation using software introduced in the next paragraph (flexImaging and SCiLS Lab).

2.3.4. Data analysis

IMS ion images were generated using flexImaging v. 5.0 software (Bruker) and SCiLS Lab v. 2016b software (Bruker) with data normalized to the total ion count (TIC). Acquired spectra were also exported from flexImaging into mMass, an open-source mass spectrometry tool (Strohalm et al., 2010) to display global spectra acquired from mouse and patient testicle samples.

2.3.4.1. Comparing spectral properties

For comparisons of peak number, average intensity and signal to noise (S/N) ratio, the TIC normalized average spectra of each measured testicle section were exported as CSV file to mMass. Here peak picking of spectra was conducted with S/N 2, relative intensity threshold 0.5%, picking height 90% and applied baseline, smoothing and deisotoping. The average peak number, intensity and S/N ratio from three technical replicates per group were plotted with mean ± SE.

2.3.4.2. Spatial Segmentation

A spatial segmentation pipeline was conducted in SCiLS on the acquired IMS data from clinical samples for unbiased hierarchical clustering with a minimal interval width of ± 0.07 Da for recognition of the distribution pattern of ions. The raw spectra were preprocessed by using the top hat baseline removal algorithm. Furthermore, the total ion count (TIC) normalization and medium denoising were applied using the segmentation pipeline. The resulting clusters, consisting of spectra grouped together based on their statistical spectral similarity, were manually examined to visually correlate their spatial patterns with histological features of the tissue sample. Moreover, all spectra within a particular cluster are assigned a selected pseudo-color and displayed as a spatial segmentation map in which pixels are color-coded according to their cluster assignment (regions of distinct molecular composition) (Alexandrov, 2012). Afterward, the clusters representing relevant regions of interest were selected for further analysis. Using the SCiLS

Lab tool 'Find discriminative *m/z* values', peptide *m/z* values were obtained from the spatial segmentation map by discriminating between each of the clusters. This tool uses the receiver operating characteristic (ROC) curve analysis to quantify how well a selected *m/z* value discriminates between two different states. Following the ROC curve analysis, the resulting mass lists (*m/z* values) providing an area under the curve (AUC) > 0.70 were considered to be significantly discriminative and were exported as an excel file and further processed through the in-house developed program (as described in the 2.5.1.)

2.4. Liquid chromatography – mass spectrometry

After the *m/z* value lists of interest have been delivered by computational analysis of a MALDI IMS dataset, they have to be associated with their molecular identities. In order to do so, follow-up peptide identification was performed using the MS-based proteomic method: LC-MS.

2.4.1. Sample preparation

Three technical replicates, each containing three adjacent tissue sections of 12 μm, were prepared from each testicular biopsy (n=6) amounting to 18 individual samples. Besides the analysis of the individual samples, two sets of sample pools were generated and analyzed. To concentrate the samples and achieve higher protein yield and identification using LC-MS, technical replicates from the same testicular biopsy were pooled together to constitute a pool from one biological sample. Sample pool A included six pooled samples made by mixing together aliquots from three technical replicates originating from the same testicular biopsy. On the other hand, sample pool B consisted of three pooled samples made by mixing aliquots of one technical replicate per biopsy. An additional pool was made that combined aliquots from all samples from pools A and B (Table 2).

Table 2: Experimental design of LC-MS experiment**.** There were three sample groups used in this study: individual samples, sample pool A and sample pool B. Individual samples consisted of three technical replicates generated from each testicular biopsy. Sample pool A included six pooled samples made by combining aliquots from three technical replicates originating from the same testicular FFPE block. Sample pool B included three pooled samples made by mixing aliquots from one technical replicate per biopsy. The entire pool consisted of aliquots from all pooled samples. All individual samples and pools were used for protein identification using the MaxQuant software.

	Preserved spermatogenesis	Mixed atrophy 1	Mixed atrophy 2 biopsy a	Mixed atrophy 2 biopsy b	Spermatogenic arrest biopsy a	Spermatogenic arrest biopsy b	Sample pool B
	PS1.1	MA1.1	MA2a.1	MA2b.1	SA1a.1	SA1b.1	Pool P.1
	PS1.2	MA1.2	MA2a.2	MA2b.2	SA1a.2	SA1b.2	Pool P.2
	PS1.3	MA1.3	MA2a.3	MA2b.3	SA1a.3	SA1b.3	Pool P.3
Sample pool A	Pool PS1	Pool MA1	Pool MA2a	Pool MA2b	Pool SA1a	Pool SA1b	Entire pool: Pool all

FFPE sample preparation for LC-MS was done according to the PreOmics iST FFPE Sample Preparation Kit using manufacturer's protocol. The protocol consists of three steps: cell lysis, protein digestion and purification of peptides.

Briefly, a range of MS-compatible buffers was used in order to efficiently reverse formalin crosslinks and extract and solubilize proteins for following LC-MS analysis. Firstly, the tissue was incubated with "Lysis" buffer at 95°C for one hour in order to facilitate tissue lysis and protein denaturation, reduction and alkylation. Additionally, samples were sonicated in order to shear the DNA from the sample. Next, lysate was incubated with "Digest" solution containing Trypsin and LysC at 37°C for three hours in order to ensure protein digestion. Thirdly, the homogenate was purified from hydrophobic and hydrophilic contaminants implementing several wash steps. Following elution of the peptides from the cartridge to the collecting tube, samples were thoroughly dried in a speed vac (Thermo) before they were re-dissolved in "LC-Load" solution.

Following the preliminary measurements with low protein yield and identification, the protocol adjustment was applied. It consisted of performing the first two sample preparation

steps, tissue lysis and protein digestion, in Eppendorf vials instead of cartridges to prevent the sample loss that would otherwise occur.

2.4.2. MS measurement

Samples were injected in an Ultimate 3000 RSLCnano system (Thermo) separated in a 25-cm Aurora column (Ionopticks) with a 50-min gradient from 6 to 43% of 80% acetonitrile in 0.1% formic acid. The effluent from the HPLC was directly electrosprayed into an Orbitrap Exploris 480 (Thermo) operated in data-dependent mode to automatically switch between full scan MS and MS/MS acquisition. Survey full scan MS spectra (from *m/z* 350–1400) were acquired with resolution R=60,000 at *m/z* 400 (AGC target of $3x10^6$). The 15 most intense peptide ions with charge states between 2 and 6 were sequentially isolated to a target value of $2x10^5$, and fragmented at 30% normalized collision energy and acquired with resolution R=15,000 at *m/z* 400. Typical mass spectrometric conditions were: spray voltage, 1.5 kV; no sheath and auxiliary gas flow; heated capillary temperature, 275°C; ion selection intensity threshold, $5x10^3$ counts.

2.4.3. Data analysis

Protein identification was performed by MaxQuant 1.6.0.16 software package. Parent ion and fragment mass tolerances were 8 ppm and 0.7 Da respectively and allowance for two missed cleavages was made. Human canonical protein database from Uniprot (release June, 2018), filtered to retain only the reviewed entries was used for the searches of the clinical samples. Regular MaxQuant conditions were the following: Peptide FDR, 0.01; Protein FDR, 0.01; Min. peptide Length, 5; Variable modifications, Oxidation (M); Acetyl (Protein N-term); Acetyl (K); Dimethyl (KR); Fixed modifications, Carbamidomethyl (C); Peptides for protein quantitation, razor and unique; Min. peptides, 2; Min. ratio count, 2. Proteins were validated on the basis of at least 1 unique peptide detected in the proteome of all the 3 replicates or in at least 2 of the 3 replicates.

2.4.3.1. Statistical analysis

In order to detect significant changes in protein levels between control and patient samples, statistical analysis on the acquired LC-MS/MS data was performed. The in-house developed software, ImShot, was used for LIMMA statistical analysis. For the LIMMA test, MaxQuant proteinGroups.txt file was imported and iBAQ values were used for two-group comparison. Exclusive values were excluded, sequence coverage was set to 5% and logarithmic fold change cut-off was set to 1.

2.4.3.2. Gene ontology term analysis

The LIMMA output files were imported to ImShot software to discover biological processes of the differentially expressed proteins (DEPs) using gene ontology (GO) term analysis. A protein was considered to be expressed differentially if there was a two-fold difference (including down and up-regulation) or if it was exclusively detected in either the healthy donor or the patient tissue. In the software, the background was set to Default (Reactome database) and the p-value was adjusted to Bonferroni-Hochberg after the over-representation test.

2.5. Combining LC-MS and MALDI IMS datasets

2.5.1. Identification of peptide masses

The ImShot software was used for systematic matching of spatially resolved peptide masses from MALDI IMS with their corresponding identified proteins in LC-MS. The software algorithm pre-processed both IMS and LC-MS raw data to filter out potential contaminants (LC-MS) and create a monoisotopic mass list (IMS). The deisotoping algorithm, using standard tolerances (±0.15 Da), was applied on the IMS mass lists which were acquired from SCiLS Lab that segregated the entire IMS dataset into its component spatial clusters (explained in chapter 2.3.4.2.). On the resulting mass lists, the peak correction algorithm was applied.

In order to generate the LC-MS mass list, previously explained LIMMA statistics (chapter 2.4.3.1.) was applied to the LC–MS peptide data. For this analysis, peptideGroups.txt output

file and intensity values were used. Each mass in the deisotoped IMS mass list was then matched with the LC–MS peptide masses within an appropriate tolerance τ (± 0.1 Da in this case). Additionally, if the comparison resulted in an ambiguous assessment of *m/z* values from IMS to several peptides identified in the LC–MS analysis, such peptides had to be ranked according to the scoring system termed as "most likely peptide (MLP) score". A particular *m/z* value from IMS was then assigned to that identified peptide (from LC–MS analysis), which had the highest MLP score (Lahiri et al., 2021).

2.5.2. Gene ontology term analysis

To find the biological processes represented by the identified proteins *in situ*, GO term analysis was performed using previously mentioned Imshot software. For this analysis, all identified proteins contained in each cluster were used. Other settings were the same as the ones mentioned in chapter 2.4.3.2.

3. Results

3.1. Optimization of MALDI imaging protocol for studying FFPE tissues

3.1.1. Establishment and quality assessment of sample preparation protocol

The first objective of this study was to develop a reliable and reproducible workflow for MALDI IMS peptide analysis of FFPE tissues. A schematic overview of the sample preparation steps is outlined in Figure 3, from which we identified "Antigen retrieval", "*In situ* digestion" and "Matrix deposition" as the most crucial parameters required for the preservation of tissue morphology and analyte localization, while obtaining abundant peptide signal intensities. To achieve this, various conditions were tested on mouse testis samples before proceeding with the pilot study using clinical human testis samples.

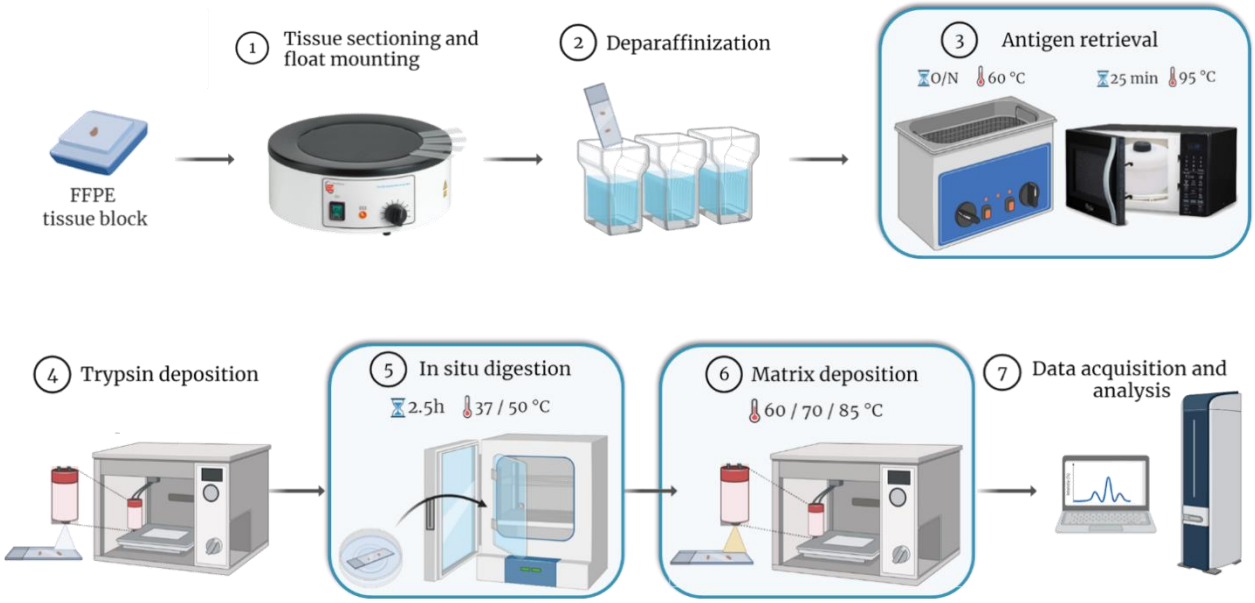

Figure 3. Schematic overview of the sample preparation workflow for peptide MALDI TOF IMS of FFPE samples. Steps that were optimized within the framework developed herein are highlighted in blue squares, with tested conditions listed within (created with Biorender.com free version)

To investigate the effect of AR step on MALDI IMS mass signals, two protocols were analyzed: a) OI (16-18h) in a water bath set up at 60°C and b) HP microwave cooker set up at 400W and 800W (Figure 3, panel 3).

The effects of increasing temperatures in the *in situ* digestion and matrix deposition steps were subsequently analyzed with the aim to optimize peptide count and intensity while preserving analyte localization. For on-tissue digestion step 37°C and 50°C temperatures were compared. The 37°C temperature was used according to the recommendation of Judd et al. (2019), while 50°C is a commercially used tissue digestion temperature (Figure 3, panel 5). In the matrix deposition step, three sprayer nozzle temperatures were compared: 85°C, 70°C and 60°C (Figure 3, panel 6). However, high nozzle temperature (85°C) caused non-uniform matrix deposition and therefore, lower nozzle temperatures were further tested and compared.

Additionally, the effect of different chemical compositions of trypsin solution for enzymatic digestion of tissue proteins was analyzed: a) 74 µg/mL of trypsin dissolved in 100 mM NH_4HCO_3 and 9% ACN (Judd et al., 2019) and b) 25 µg/mL of trypsin dissolved in 20 mM NH_4HCO_3 and 0.01% glycerol (Ly et al., 2019) (Figure 3, panel 4). For the optimum amount of trypsin per unit area of the tissue, we used the solution proposed by Judd et al. (2019) in all further measurements.

3.1.1.1. Evaluation of IMS spectral properties

In order to evaluate and determine the effect of the above-mentioned conditions, we first compared the MALDI IMS spectral properties using mouse testis tissue sections (Figure 4). All measurements were repeated two times using the serial section of the same FFPE tissue block.

For the AR step, the HP method yielded a lower number of ion peaks under different conditions, as compared to OI. However, the S/N ratio and intensity were higher in the HP AR method. Upon using higher on-tissue digestion temperature (50°C), a higher number of peptide peaks (Figure 4A) and lower S/N ratio and intensity values were observed (Figure 4B-C). The same trend of higher peptide peak count and lower S/N ratio and intensity values was observed when using 70°C matrix deposition temperature. Therefore, the sample processed with higher *in situ* digestion (50°C) and matrix deposition temperature (70°C) led to the highest number of ion peaks (236 individual *m/z* values) in the case of OI, whereas the number was lower (60) in the case of HP AR method (Figure 4A).

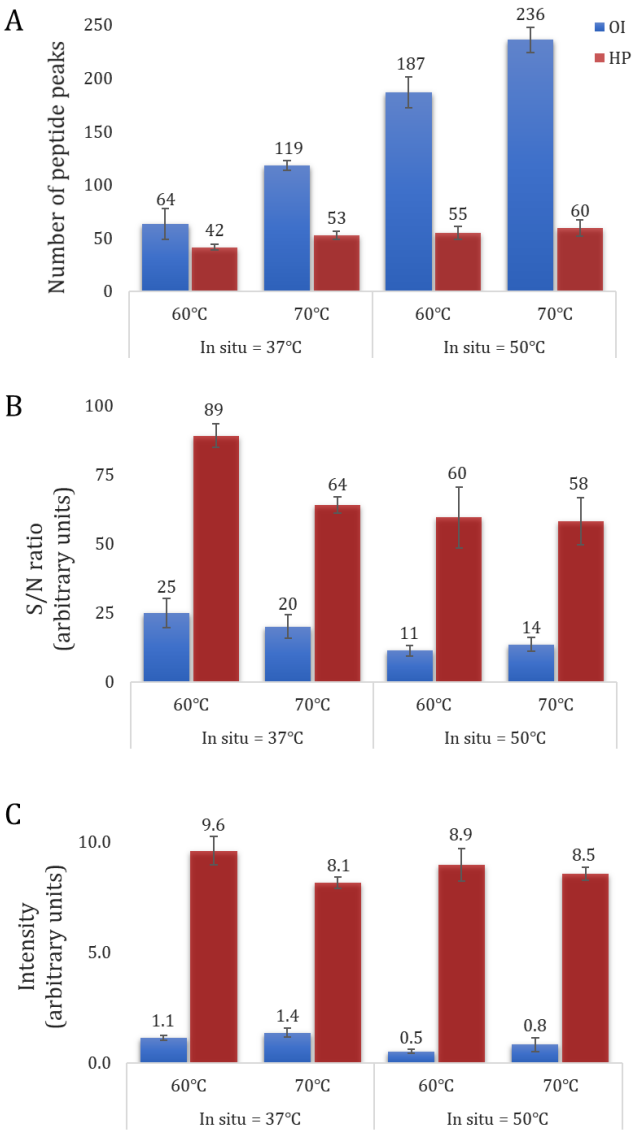

Figure 4. Evaluation and comparison of MALDI IMS spectral properties of mouse testis FFPE samples processed with different AR (OI and HP), *in situ* digestion (37°C and 50°C) and matrix deposition (60°C and 70°C) conditions. Following spectral properties were compared: (A) peak number, (B) the S/N ratio and (C) intensity expressed in arbitrary units. S/N and intensity values represent the mean of S/N and intensity of all peaks detected per measured tissue sample. Error bars represent standard error from two technical replicates of mouse testis FFPE samples. For each condition, experiments were repeated independently using consecutive sections of the same tissue block.

3.1.1.2. Comparative analysis of the spatial distribution

To further assess the efficacy of each condition, the spatial distributions of peptides in several ion images were compared to histological features in a post-measurement H&E stained tissue section (Figure 5). This qualitative analysis of MALDI ion images was shown only for OI AR technique. Here, the lower matrix deposition temperature (60°C) resulted in analyte delocalization across the tissue section (Figure 5B, i-ii) as compared to higher matrix deposition temperature (70°C) (Figure 5B, iii-iv). The lower trypsin digestion temperature (37°C) in combination with higher matrix deposition temperature (70°C) maintained *in situ* analyte spatial distribution throughout the tissue section (Figure 5B, iii). The higher digestion temperature (50°C) resulted in reduced peptide ion intensity and increased background intensity, mainly on the corners of the tissue section (Figure 5B, iv).

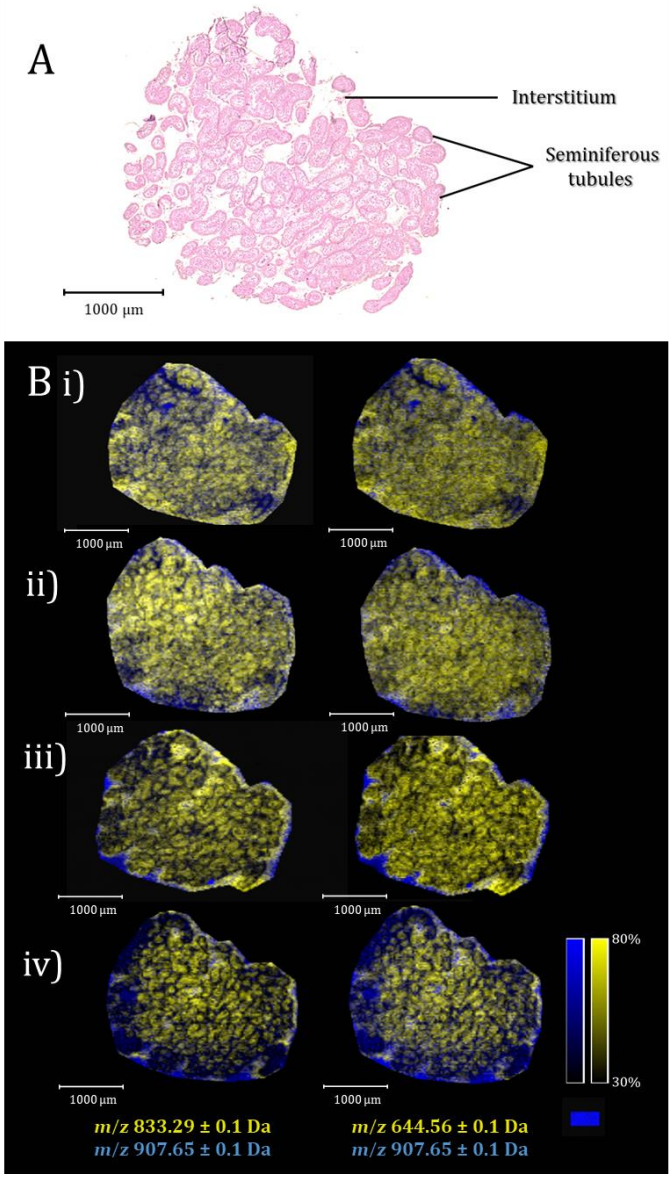

Figure 5. Comparative analysis of the spatial distribution of two MALDI sample preparation optimization steps involving *in situ* digestion (37°C and 50°C) and matrix deposition temperature (60°C and 70°C) assessment. (A) Optical image of the H&E stained tissue section after IMS measurement. (B) MALDI ion images resulting from different on-tissue digestion and matrix deposition temperatures: (i) digestion temp. 37°C, matrix deposition temp. 60°C, (ii) 50°C, 60°C, (iii) 37°C, 70°C and (iv) 50°C, 70°C. Overlaid ion images on the left side show *m/z* 833.29 ± 0.1 Da (yellow) corresponding to seminiferous tubules and *m/z* 907.65 ± 0.1 Da (blue) corresponding to the background. Overlaid ion images from the right side show the same distribution of *m/z* 644.56 ± 0.1 Da (yellow) in tubules and *m/z* 907.65 ± 0.1 Da (blue) in the background. The spatial intensity distribution of the selected peptide ions was displayed using a color code. The ion intensity bar is present on the right side of the figure. Scale bars - 1000 µm.

3.1.2. Testing the optimized protocol for potential application on human testicular biopsies

Following the systematic testing and optimization of key parameters, the established workflow was applied on human testicular samples for translating the findings to a clinical setting. The analyzed samples belonged to three morphologically different groups: PS, MA and SA.

Optimized sample preparation conditions used in all further measurements were following: OI (16-18h) at 60°C, trypsin without glycerol, lower *in situ* digestion temperature (37°C) and higher matrix deposition temperature (50°C).

3.1.2.1. Evaluation of IMS data reproducibility

First, the reproducibility of MALDI IMS raw data was evaluated by plotting the average spectra of *m/z* region 1084.0 to 1092.0 of four independently measured serial sections. Sections belonging to the FFPE testicular biopsy of MA2 patient were prepared and measured independently on four different days (Figure 6). Spectra generated from repeated experiments were highly reproducible with no systematic mass shifts or observable differences detected in peak intensities between duplicates.

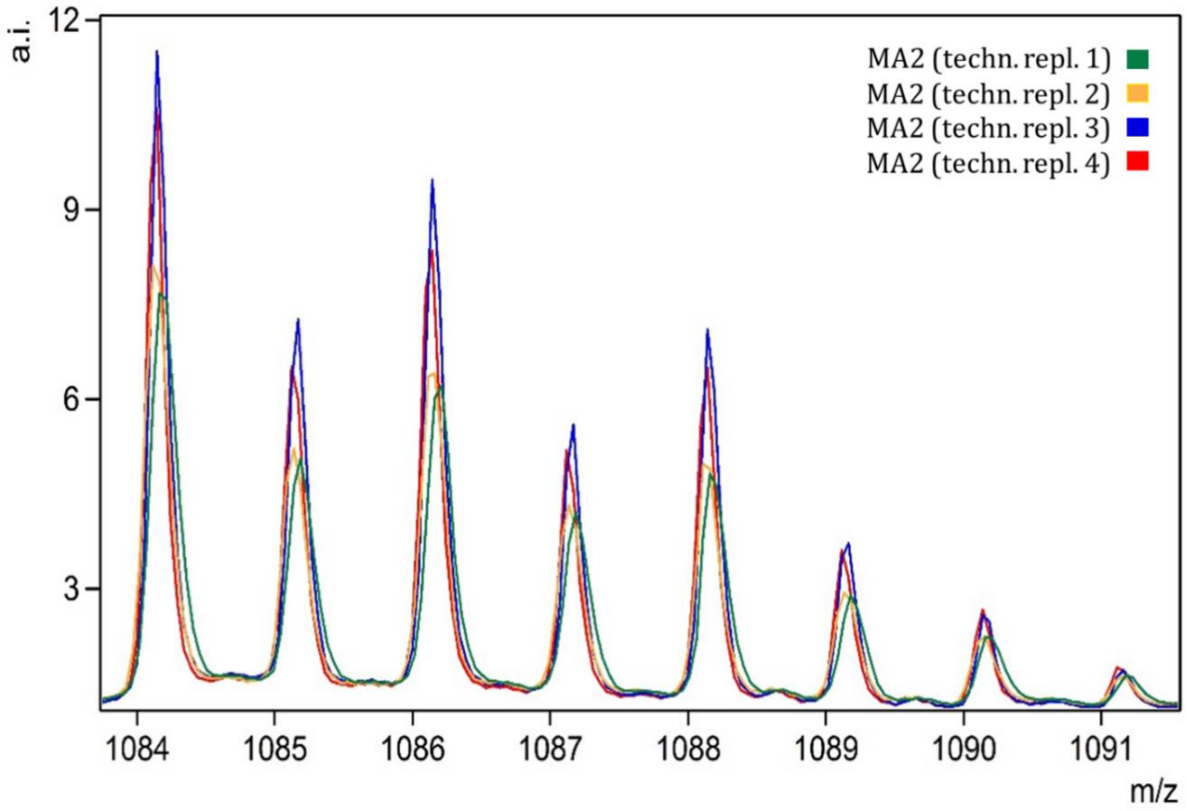

Figure 6. Evaluation of MALDI IMS data reproducibility by plotting average spectra of *m/z* region 1084.0 to 1092.0 and displaying four technical replicates of MA2. Spectra were displayed without normalization. The spread of the single spectral intensities is indicated in bars; a.i. - arbitrary intensity

3.1.2.2. Evaluation of MALDI IMS spectral properties

The spectrum quality check was done by evaluating and comparing MALDI IMS spectral properties between tissues belonging to four human tissue donors (Figure 7). As it can be seen from Figure 7, the overall peak number varied from 74 to 98 across the patient samples, while the S/N ratio was well above 14 and peak intensity above 8. The values here corroborated well with those from mouse testis under similar conditions (Figure 4). Results confirmed the applicability of the method to tissues derived from independent sources as well as the reproducibility and stability of the spectral properties when applying this protocol.

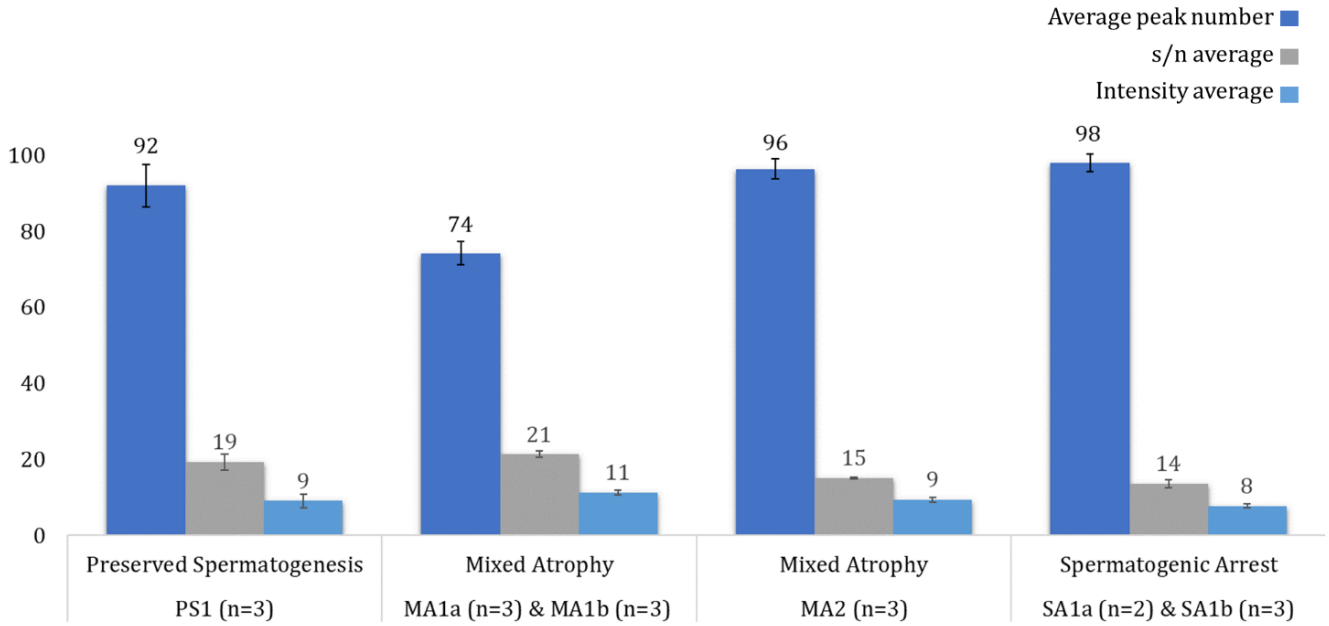

Figure 7. MALDI IMS spectral properties of clinical testis FFPE samples. Overview of peptide peak number, the S/N ratio and the intensity. Error bars represent standard error from three to five technical replicates of patient FFPE samples. PS1 – biopsy from patient belonging to preserved spermatogenesis group; MA1a,b – two biopsies taken from patient 1 of mixed atrophy group; MA2 biopsy taken from patient 2 of mixed atrophy group; SA1a,b – twp testicular biopsies derived from patient with spermatogenic arrest

3.1.2.3. Comparative analysis of the spatial distribution

To examine if peptides maintain their original location on the tissues, correlative analysis of MALDI ion images was conducted showing spatial distributions of three *m/z* species (as representative peptides) in correlation with post-measurement H&E stained section used to assess the histopathology of the tissue (Figure 8). The representative mass signals were chosen for their distinctive distribution in the tissue that corresponds to different testicular compartments (Figure 8B). The H&E staining on the same tissue section revealed that *m/z* 624.23 corresponds to seminiferous tubules while *m/z* 908.14 corresponds to the interstitial spaces (Figure 8B, i-ii). Additionally, *m/z* 908.14 was used as a representative mass of the background area (Figure 8B, iii). Overlaid representation of previously mentioned ion images with H&E stained section was shown for improved visualization of testicular morphology (Figure 8C). These results correlated the peptide distribution patterns with testicular morphology highlighting the structural differences between seminiferous tubules and interstitial spaces from background areas. They also demonstrated the feasibility of this protocol to clearly distinguish and resolve individual anatomical features in complex human FFPE tissue samples (testicular tissue in this case).

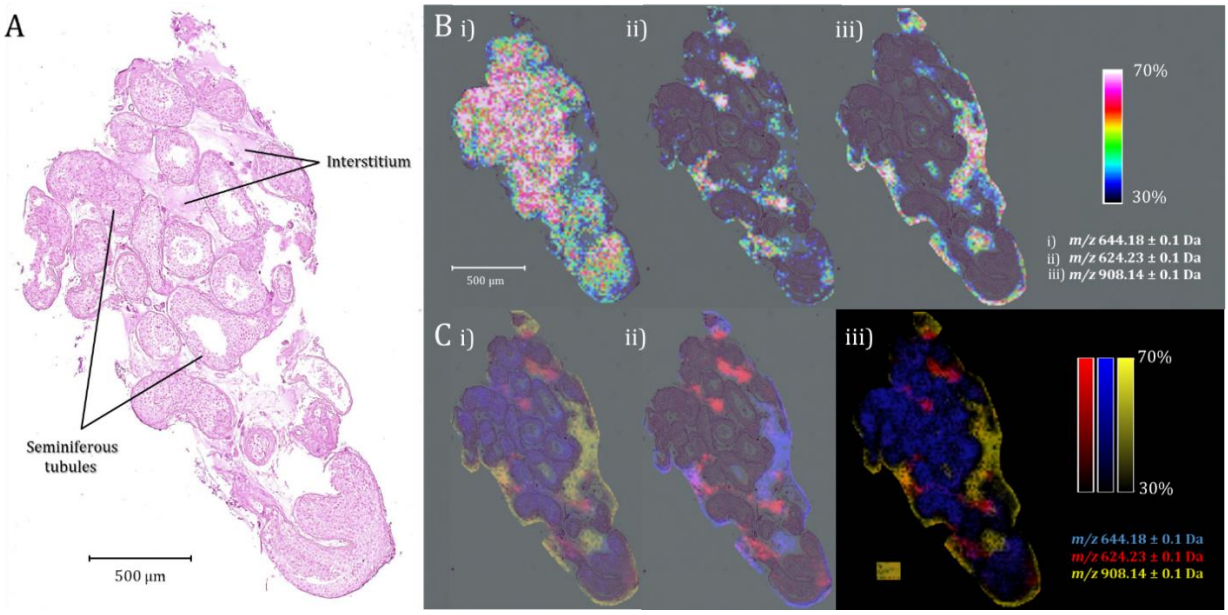

Figure 8. Spatial distributions of different *m/z* species are highly conserved in FFPE tissue samples prepared with optimized sample preparation protocol. Representative measurement of preserved spermatogenesis tissue section was previewed. (A) Post-measurement H&E stained human testis sample. (B) Representative MALDI IMS ion images of i) *m/z* 624.23 ± 0.1 Da corresponding to seminiferous tubules, ii) *m/z* 908.14 ± 0.1 Da corresponding to the interstitial spaces and iii) *m/z* 908.14 ± 0.1 Da that shows background area. (C) Overlaid images of the preceding ion images showing the individual localization of the ion signals where i) represents an overlay of all *m/z* species from (B) and H&E stained section (A), ii) represents an overlay of (B) ii) and iii) ion images with H&E (A) for better interstitial visualization and iii) shows the same overlay as in (C, i) with higher contrast. The ion intensity bar is present on the right side of the figure. Scale bar - 500 µm.

3.2. LC-MS analysis

Proteomic profiles of testicular samples from patients diagnosed with different types of idiopathic infertility (MA and SA) were obtained and compared to that of fertile donors with PS.

Following preliminary sample preparation and measurement (Figure 9, red columns), technical optimization of different sample preparation steps was performed. To further ensure higher protein yield and identification by LC-MS, sample pools were measured. After mentioned adjustments, at least 1811 unique proteins were identified per patient. Although the number of identified proteins appears to be low as compared to shotgun proteomics experiments, they were actually identified from very low input materials. The average input volume of the patient biopsies was of the order of 10^6 μm^3.

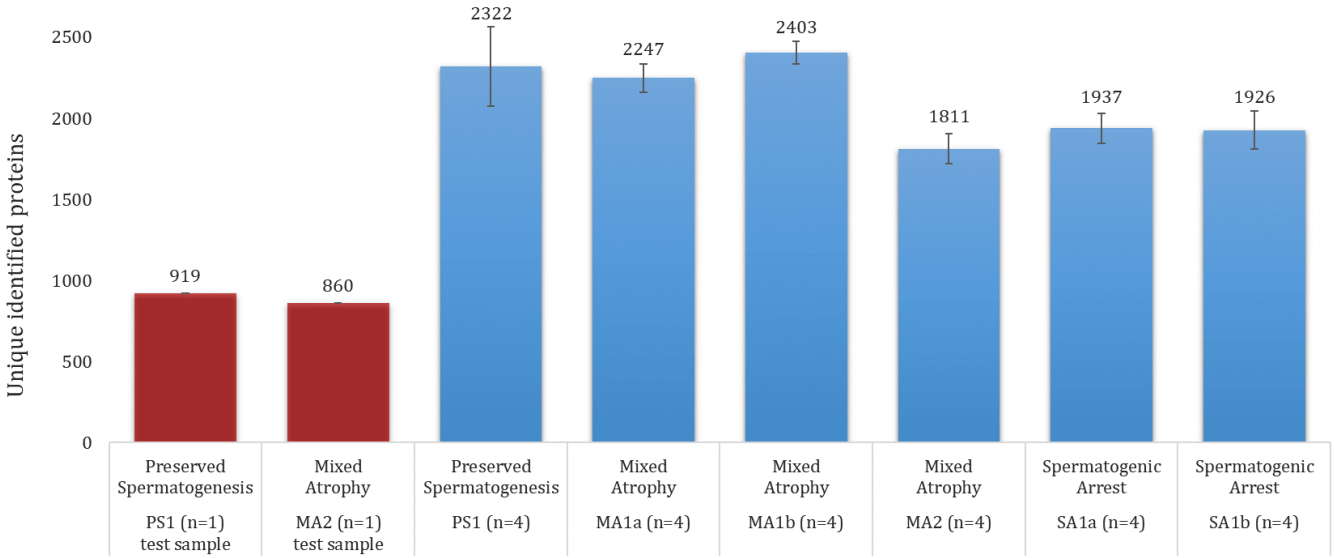

Figure 9. The number of unique identified proteins determined by LC–MS/MS analysis of clinical testis FFPE samples. The red-colored columns represent test measurement after which optimization steps were developed and applied to further measurements of clinical samples (blue-colored columns). Error bars represent standard error from four technical replicates of one FFPE sample. PS1 – testicular biopsy derived from fertile donor with preserved spermatogenesis; MA1a – first testicular biopsy derived from first patient with mixed atrophy; MA1b – second testicular biopsy derived from first patient with mixed atrophy; MA2 – testicular biopsy derived from second patient with mixed atrophy; SA1a – first testicular biopsy derived from patient with spermatogenic arrest; SA1b - second testicular biopsy derived from patient with spermatogenic arrest

3.2.1. Proteomics of human biopsies from idiopathic infertile men

LC-MS/MS analysis of atrophied patients identified a total of 1817 proteins, out of which a total of 1668 proteins were common with fertile donor and 101 and 48 proteins were exclusively detected in the testis of the patient and healthy donor respectively (Figure 10A). Limma statistical analysis of the shared 1668 proteins showed that 163 proteins were highly upregulated in the MA group as compared to 168 proteins that were prominently downregulated (> two or < -two fold change in at least 3 out of 4 technical replicates) (Figure 10C, brown and blue filled circles beyond vertical dotted lines). In the case of SA, a total of 1776 proteins were identified with 1537 shared and 209 proteins that were unique to the healthy tissue as compared to 30 that were exclusively detected within the diseased testis (Figure 10B). Here, we observed that 314 and 267 proteins were highly up- or downregulated respectively in the analyzed tissues (Figure 10D, brown and blue filled circles beyond vertical dotted lines). Among the identified proteins, 480 were detected as DEPs between MA and control group and 820 between SA and control group (Figure 10E).

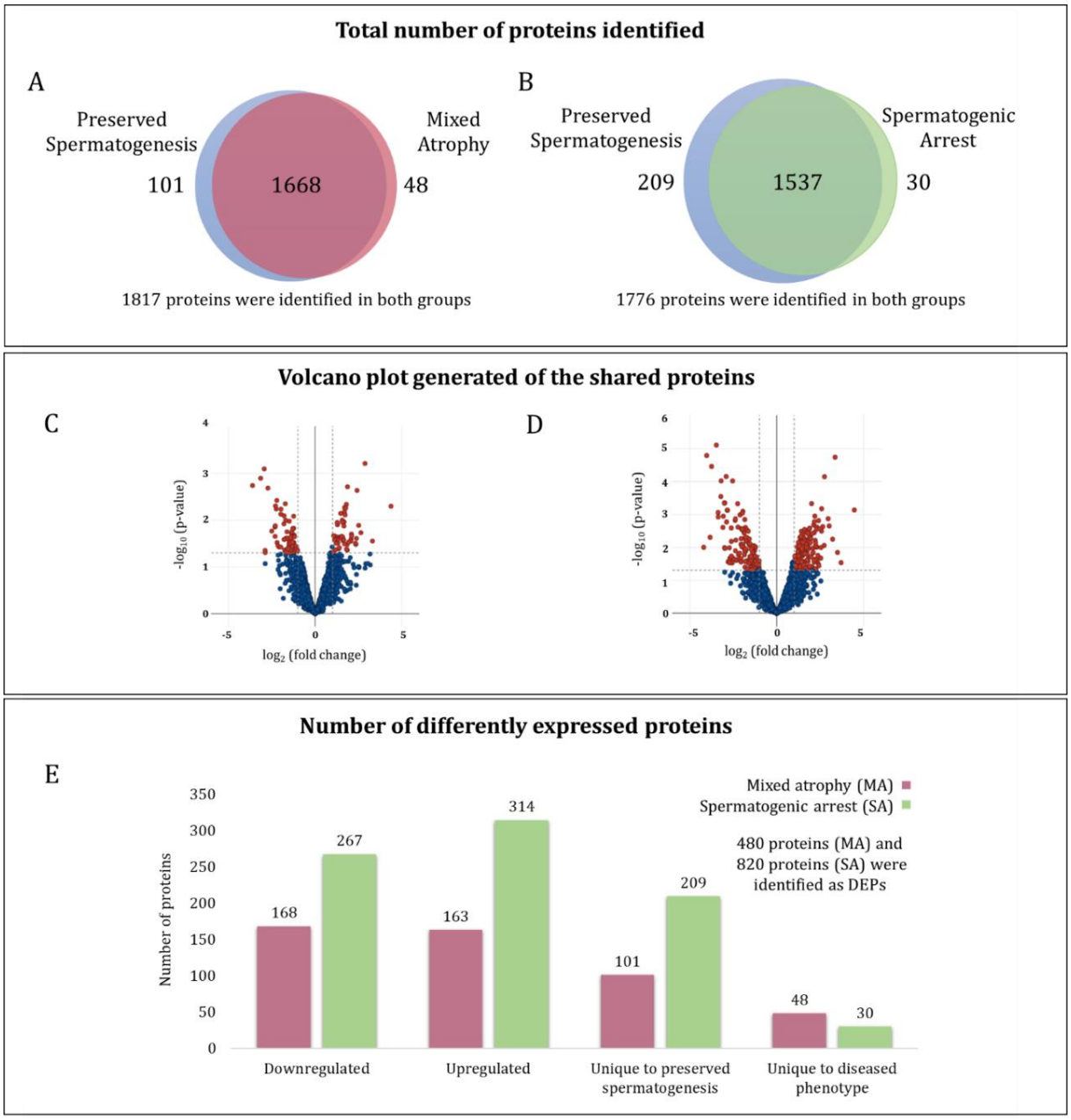

Figure 10. Proteomic analysis of the testis tissue of three groups: PS, MA and SA. Venn diagram of identified proteins showing exclusive and shared proteins between the fertile donor (PS) and patient tissue of (A) mixed atrophy and (B) spermatogenic arrest group. (C-D) The panel showing a Volcano plot with the distribution of shared proteins after statistical analysis by LIMMA moderated t-test. The filled brown circles represent the statistically significant proteins in both control (negative fold change) and the infertility group (positive fold change). (E) Differentially expressed proteins of experimental groups (MA and SA).

3.2.2. Gene ontology analysis of dysregulated proteins

To identify the dysregulated cellular processes under different idiopathic conditions, the biological processes that were represented by the most misregulated proteins (both shared and exclusive) were analyzed. Per condition, the top seven statistically significant biological processes are displayed (Figure 11, 12).

3.2.2.1. Mixed atrophy group

The GO term analysis of the DEPs of the MA group revealed that the most significantly upregulated biological processes were mostly hemorrhage-related, such as platelet degranulation, blood coagulation, fibrin clot formation and hemostasis which insinuates the presence of damaged blood vessels (Figure 11B). In addition, upregulation of immune response factors that contribute to neutrophil degranulation and activation involved in immune response was observed. Upregulation of those factors was previously associated with subfertile and infertile pathologies (Hussein et al., 2005). Other highly upregulated GO terms included the hydrogen peroxide catabolic process that suggested the presence of oxidative stress in the tissues, and negative regulation of chromatin silencing that involves the upregulation of many histone H1 variants (H1-0, H1-5, H1-2, H1-6).

Moreover, the GO term analysis revealed that translation-related processes such as mRNA and RNA splicing and regulation of mRNA metabolic process were the most downregulated ones. Additionally, downregulation of the G2/M phase transition process suggested possible mitotic dysregulation in impaired tubules of patients with MA (Figure 11A).

The proteins detected exclusively in either MA or control testis also provide valuable insights into the most predominant dysregulated biological processes (Figure 11C-D). Exclusive proteins in MA patients were involved in the signaling pathways such as adenylate cyclase-inhibiting G protein-coupled receptor signaling pathway that leads to a decrease in the concentration of cyclic AMP (cAMP) (Figure 11D). Since cAMP plays a central role in cell signaling during sperm differentiation and maturation, decreasing its level could lead to the infertile phenotype related to defects in sperm motility and capacitation (Buffone et al., 2014). This substantiates the enrichment of sperm motility and capacitation in the healthy

donor. Furthermore, proteins related to neurotransmission and signaling were also exclusively found in the testis tissue of patients with MA. The most upregulated ones contributed to modulation of chemical synaptic transmission, regulation of trans-synaptic signaling, neurotransmitter transport, regulation of neurotransmitter levels and synaptic vesicle priming.

The GO term analysis of the fertile donor with functional spermatogenesis revealed the participation of exclusive proteins ENO3, GAPDH and SERPINA12 in the gluconeogenesis signaling pathway that is present in spermatogonia during spermatogenesis (Park & Pang, 2021) (Figure 11C). Other exclusive proteins included ones that are involved in cellular regulatory pathways such as regulation of protein autophosphorylation, regulation of protein-containing complex assembly, positive regulation of endopeptidase activity as well as in metabolism-related ones (branched-chain amino acid catabolic process and small molecule catabolic process). Interestingly, some of the other significant processes such as flagellated sperm motility and sperm capacitation were also found exclusively in the control group suggesting a defective spermiogenesis process.

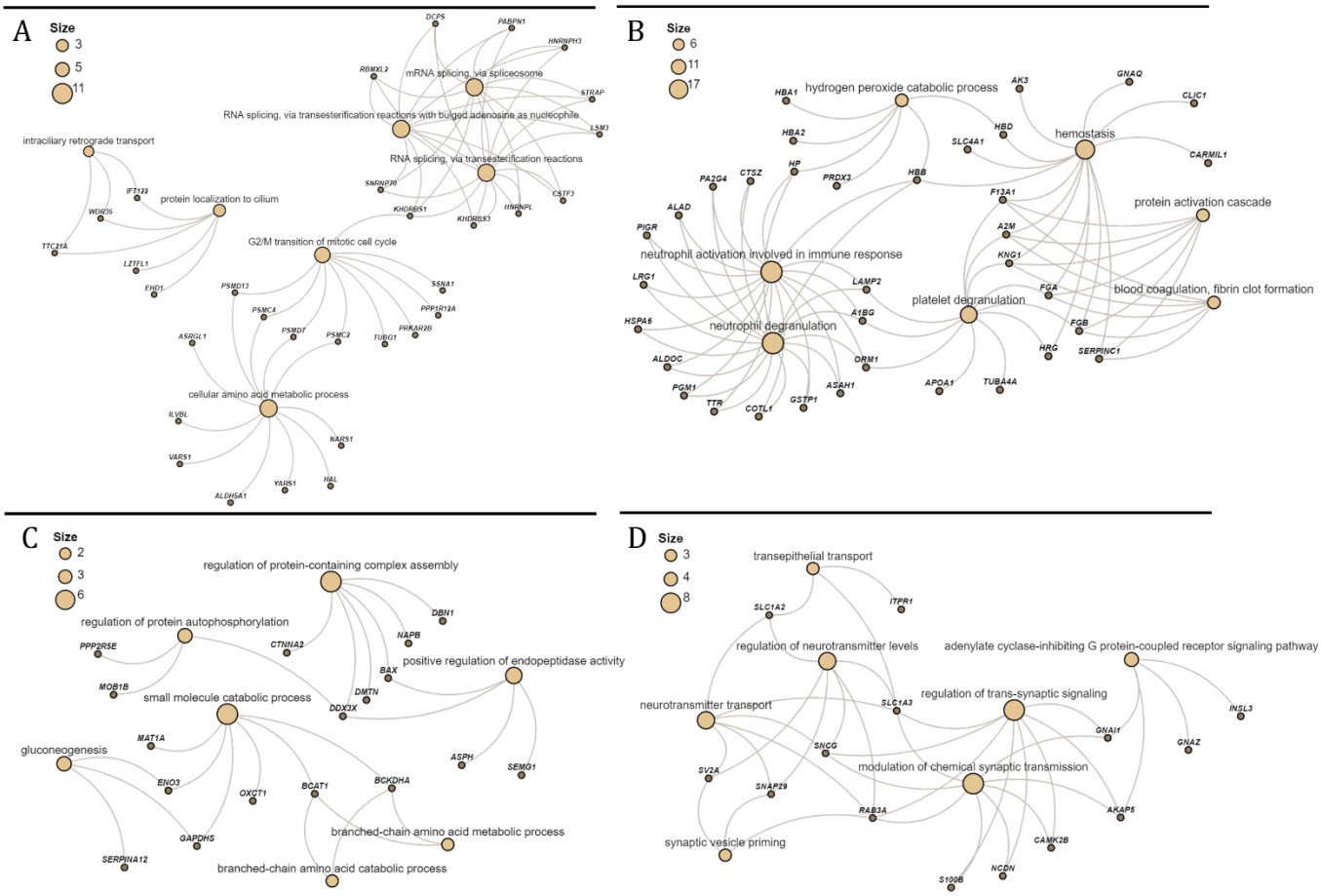

Figure 11. Altered biological processes in mixed atrophy. Gene ontology (GO) term analysis of (A) downregulated proteins, (B) upregulated proteins, (C) proteins exclusive to control and (D) proteins exclusive to MA group. The orange nodes indicate the biological processes, while the grey ones indicate the genes involved in each process. The size of the orange nodes (scale represented by numbered circle legend in the left corner) is representative of the number of genes involved in a particular biological process within the GO term map.

3.2.2.2. Spermatogenic arrest group

Similar to MA, GO term analysis of upregulated proteins (Figure 12B), from patients diagnosed with SA, revealed that the tissue was enriched with hemorrhage-related proteins participating in processes such as blood coagulation, hemostasis and coagulation, insinuating the possible damage of blood vessels and subsequent bleeding. Furthermore, SA testes demonstrated upregulation of immune response factors which are not observed in healthy conditions. Upregulation of these processes such as neutrophil activation involved in immune response and neutrophil degranulation suggested the activation of severe inflammatory and immunomodulatory activities that are linked to tissue damage or destruction. Additionally, metabolism was also affected with upregulated proteins associated with the small molecule catabolic process and organic acid catabolic process.

In addition, proteins that were significantly downregulated in SA testis was also observed. GO term analysis showed that the majority of them were involved in protein folding, positive regulation of telomerase RNA localization to Cajal body and cellular amino acid metabolic process (Figure 12A). Additionally, one of the statistically significant molecular processes, the G2/M transition of the mitotic cell cycle, was downregulated in both MA and SA group.

GO term analysis showed that the majority of proteins exclusively detected in SA testes participated in vesicle and neurotransmitter-related processes. Since the changes in neurotransmitter levels and signaling affect spermatogenesis, their substantial alterations can lead to impaired sperm production and quality (Cortés-Rodriguez et al., 2018). Interestingly, a considerable overlap of these exclusively detected biological processes was observed in MA testes tissue (Figure 12,13D).

Next, exclusive proteins identified in control samples participated in biological processes such as immune response in mucosal-associated lymphoid tissue, spermatid development, RNA transport and localization, regulation of protein polymerization and protein-containing complex localization (Figure 12C). The absence of the spermatid development process in SA tissue suggested halted self-renewal and differentiation of germ stem cell line which, in that way, interfered with late stages of spermatogenesis and fertilization. Additionally, proteins involved in the regulation of protein polymerization such as SPTB, CTNNA2, ARL2, ARFIP1,

DMTN and DBN1 have been associated with actin filament assembly and organization (Cheng & Mruk, 2012).

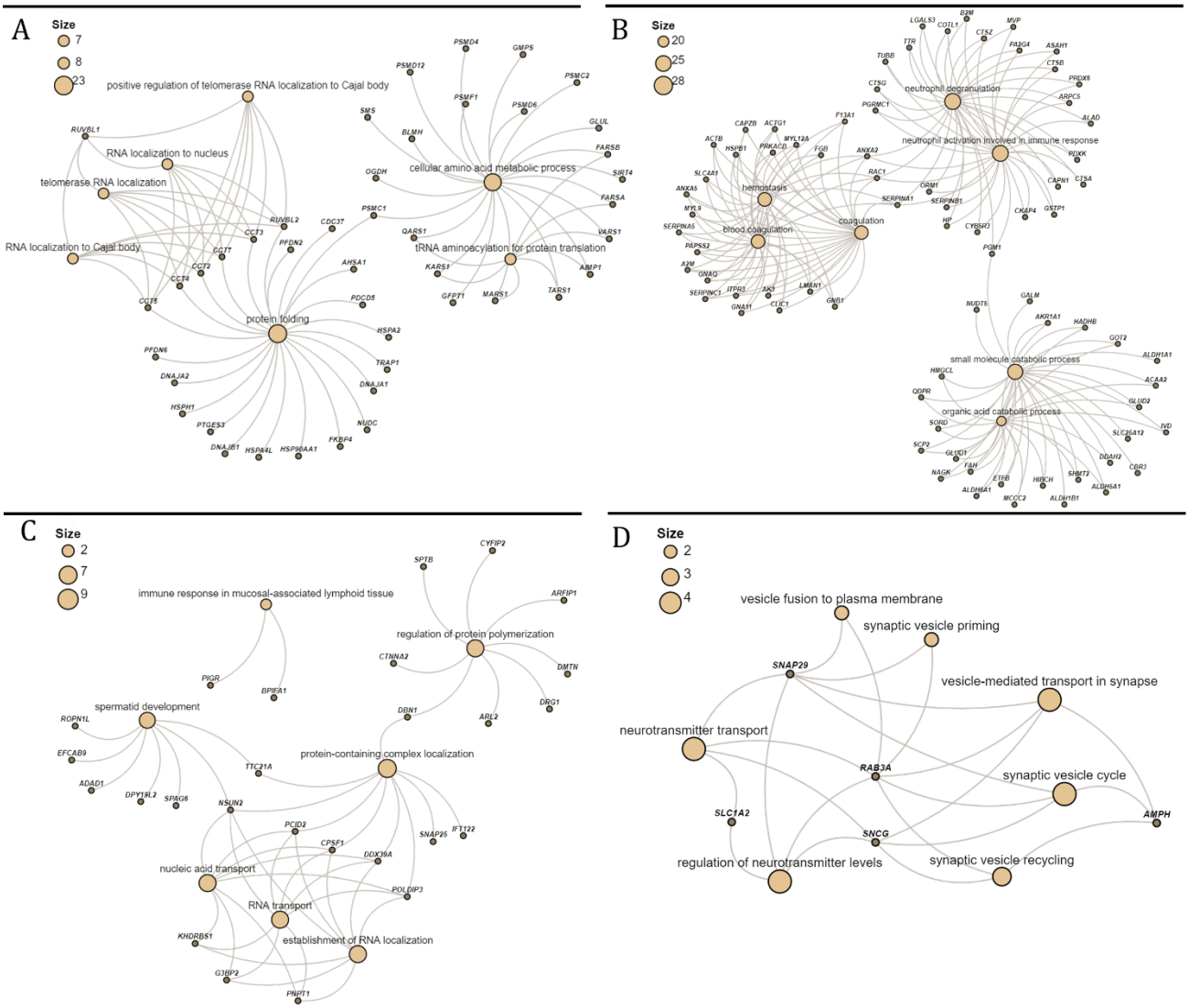

Figure 12. Altered biological processes in spermatogenic arrest. Gene ontology (GO) term analysis of (A) downregulated proteins, (B) upregulated proteins, (C) proteins exclusive to control and (D) proteins exclusive to SA group. The orange nodes indicate the biological processes, while the grey ones indicate the genes involved in each process. The size of the orange nodes (scale represented by numbered circle legend in the left corner) is representative of the number of genes involved in a particular biological process within the GO term map.

3.3. Data integration

To get a better understanding of the protein distribution and tissue compartments involved in pathophysiological changes of idiopathic infertile testes, a spatial segmentation map was generated using detected peptides from patients diagnosed with idiopathic infertility. Unbiased hierarchical clustering classified the mass spectra in the imaging data set based on spectral similarity after which the resulting tissue clusters were compared with morphological features of the tissue. Additionally, after using hierarchical clustering, the data was presented in a way that clusters containing similar spectra were shown in the same color (Mourino-Alvarez et al., 2016).

Results given in Figure 13 show two distinct types of primary clusters, in the segmentation map of all patient biopsy samples, represented mostly by the brown and lime clusters[1]. These clusters represent different morphological compartments of the testicular tissue across patient groups. In the case of the PS biopsy sample, the brown cluster represents peptides distinct to seminiferous tubules, while the lime cluster characterizes the non-tubular area, most likely the interstitial spaces (Figure 13A). In the SA1a sample, the brown cluster represents peptides localized in both tubular and interstitial areas while the lime cluster characterizes the peptides present in the Sertoli-cell-only (SCO) tubular region (Figure 13B). However, in the SA1b sample, the lime cluster contains peptides distinct to the seminiferous tubules, while the deep-blue cluster the ones localized in non-tubular, most likely the interstitial area (Figure 13C). In addition, in the MA group, MA1a and MA1b samples contain brown clusters that characterize peptides within atrophied tubules with small or no lumen, while lime ones represent the peptides localized in tubules with intact spermatogenesis (Figure 13D-E). In the MA2 sample, the cluster segmentation and histological correlation were equal to the one present in the PS sample (Figure 13F).

[1] All histological correlations with peptide signatures were annotated and confirmed by an expert pathologist.

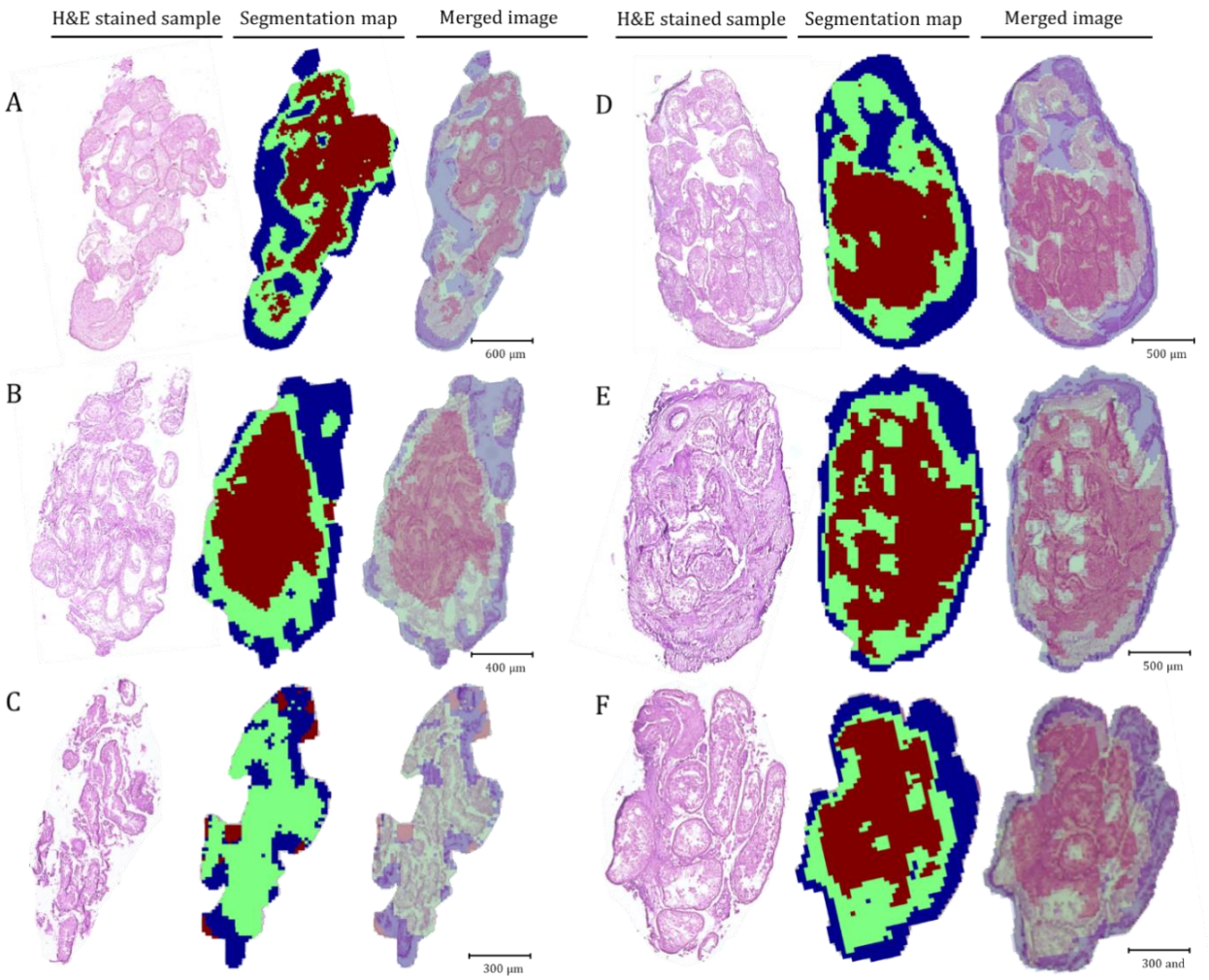

Figure 13. Segmentation proteomic map of all clinical testis samples. In the first column of each sample is the post-measurement H&E stained optical image of the sample, while in the second is its segmentation map. The third column shows the overlay of those preceding images that enables histological correlation with the cluster regions. (A) Preserved spermatogenesis sample with two distinct clusters where brown cluster represents the tubular area and the lime cluster characterizes the non-tubular area. Scale bar - 600 µm. (B) Spermatogenic arrest in spermatocyte 1 biopsy sample 1 with the brown cluster representing the tubular and interstitial area, while the lime cluster characterizes the Sertoli-cell-only tubular region. Scale bar - 400 µm. (C) Second biopsy from the same patient mentioned in (B) where the lime cluster represents tubular area and the deep-blue cluster non-tubular, most likely interstitial area. Scale bar - 300 µm. (D-E) Two biopsy samples from MA patient 1 whose brown clusters characterize atrophied tubules with small or no lumen while lime ones represent tubules with intact spermatogenesis. Scale bar - 500 µm. (F) Biopsy sample from MA patient 2 with cluster segmentation and histological correlation as in sample (A). Scale bar - 300 µm.

To identify the parent proteins of the peptides localized in different spectral clusters from Figure 13, the ImShot software was used. It successfully combined IMS and LC-MS/MS data to identify the most likely protein. Using this software, for each patient biopsy, discriminative mass lists from the above-mentioned spectral clusters were processed. However, results from two biopsies from MA1 were combined since the tissues shared the same histological correlations to molecular maps. Figures 14, 16, 18 and 20 show the identified proteins (two-fold difference in LC-MS for both up- and down-regulated proteins), belonging to each cluster, with their respective position in the volcano plot for each patient biopsy in comparison with the control group. Additionally, bioinformatic analysis of identified proteins in each cluster was carried out by GO term analysis (Figure 15, 17, 19, 21) using the same in-house built software.

3.3.1. Protein identification *in situ* for MA1 testicular samples

Using the ImShot bioinformatic pipeline, four proteins (FABP3, AKR1C1, PURA, CKB) were observed to be strongly upregulated in an atrophied tubular cluster of MA1 testicular tissue, out of which two were statistically significant in the LC-MS measurement (> two-fold difference, p-value < 0.05) (Figure 14B, right volcano plot). Dosage of these gene products has previously been shown to affect normal spermatogenesis (Oztekin et al., 2020; Park & Pang, 2021; Shen et al., 2013). The tubular cluster with normal spermatogenesis in the MA1 testis (Figure 14C, right volcano plot) showed a considerable upregulation of CA2, ALDOC, PRDX3 and SERPINC1. The fact that the aforementioned proteins have previously been shown to regulate spermatogenesis (Ryu et al., 2017; Wandernoth et al., 2015; Zhang et al., 2021), along with the fact they are localized in tubular cells, substantiates our method of data integration.

In the control tissue with preserved spermatogenesis, the most prominent peptides defining the exclusive tubular cluster were derived from ribosomal protein RPS4Y1 and ADP/ATP carrier SLC25A31 that are thought to play a role in spermatogenesis and whose expression has been shown to display an anti-apoptotic phenotype (Figure 14C, left side volcano plot). Furthermore, in the non-tubular cluster of control tissue five proteins were identified (COL6A3, COL1A1, RPS4Y1, MXRA7, PGK2, CSE1L).

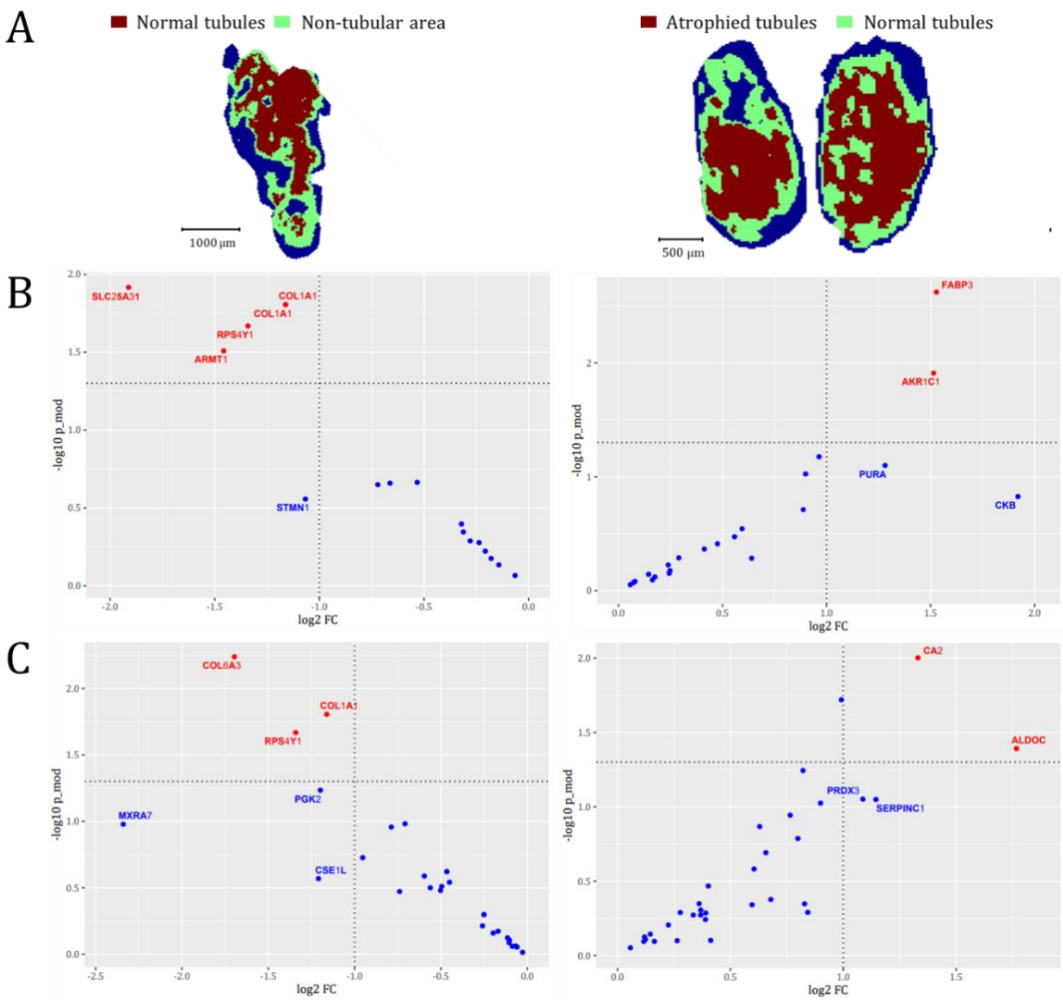

Figure 14. Protein identification *in situ* with the maximum likelihood for the MA1 testicular samples. (A) Segmentation map containing color-coded cluster legend that reflects morphological features of the tissue. (B) Part of Volcano plot that marks respective positions of the identified proteins (two-fold difference) detected in the brown cluster. (C) Same as (B) in respect to the lime cluster. Left side – proteins identified in fertile donor; right side - proteins identified in MA1 samples

3.3.2. Biological processes represented by *in situ* identified proteins from MA1

The detected biological processes of identified proteins in clusters of MA1 were summarized in Figure 15. In the atrophied tubules, identified proteins were associated with neutrophil activation involved in immune response and neutrophil degranulation processes that suggested the induction of inflammatory response (Naegelen et al., 2015) (Figure 15A). These biological processes were also observed in the GO term analysis of upregulated proteins in MA testes, identified by LC-MS (Figure 11B). Additionally, metabolism-related processes were detected consisting of aerobic respiration, cellular respiration and triglyceride metabolic pathway. On the other hand, the normal, functional tubules in MA testis consisted of proteins involved in various biosynthetic and metabolic processes such as acetyl-CoA, nucleoside bisphosphate, ribonucleoside bisphosphate and sulfur compound biosynthetic processes and fatty acid and acetyl-CoA metabolic processes (Figure 15B).

In the control tissue, proteins identified in the normal tubular cluster were involved in translation and protein folding-related processes, more specifically in chaperone-mediated protein complex assembly, protein-DNA complex assembly, regulation of protein-containing complex assembly and in the mitochondrial transport (Figure 15C). However, in the interstitial cluster, biological processes like protein localization to nucleus, protein folding and cell redox homeostasis were detected (Figure 15D).

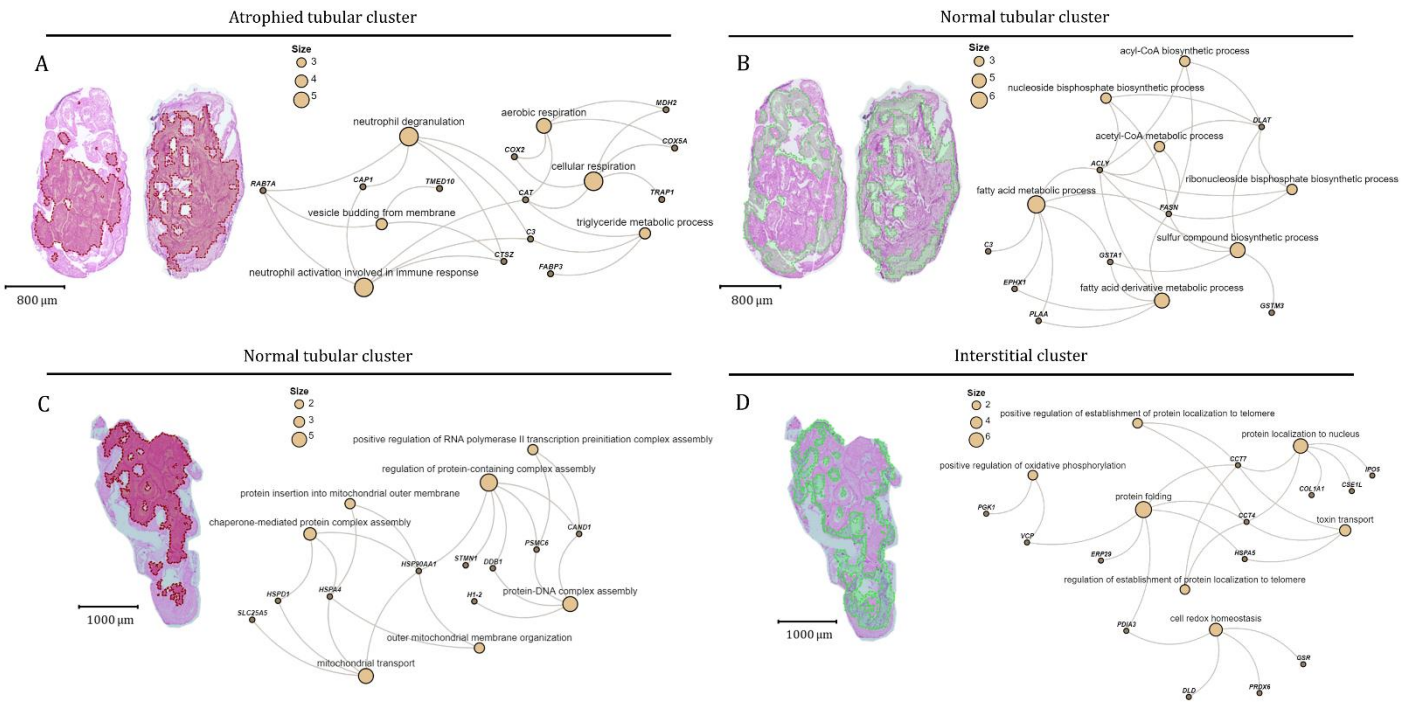

Figure 15. Gene ontology (GO) term analysis of proteins identified in each cluster of MA1 patient and control. The right side shows the overlay of segmentation map showing the cluster of interest and the H&E stained optical image of the sample, while the left side shows the GO term analysis corresponding to the cluster. Results were obtained from (A) atrophied tubular cluster and (B) normal tubular cluster of both biopsies from MA patient 1, as well as (C) normal tubular cluster and (D) interstitial cluster from fertile donor. The orange nodes indicate the biological processes, while the grey ones indicate the genes involved in each process. The size of the orange nodes (scale represented by numbered circle legend in the left corner) are representative of the number of genes involved in a particular biological process within the GO term map.

3.3.3. Protein identification *in situ* for MA2 testicular samples

In order to examine inter-patient variability, results from MA2 patient were obtained with two exclusive clusters related to tubular and non-tubular testicular areas (Figure 16-17). Three statistically significant proteins were identified in the tubular area; RAB7A, MRPL46 and CPQ (Figure 17B, right). In the non-tubular area, eight enriched proteins were detected (RAB7A, MRPL46, CPQ, AP2A1, PGAM2, CFL2, ACTB, MYH9) (Figure 17C, right). Since RAB7A, MRPL46 and CPQ are actively expressed in both spermatogenic and Leydig cells, they have been identified in both compartments.

Furthermore, in the control tissue with PS, one enriched protein was identified in the normal tubular cluster (MYCBP) while three were in the interstitial area (IPO5, CCAR2, GABARAP) (Figure 17B-C, left).

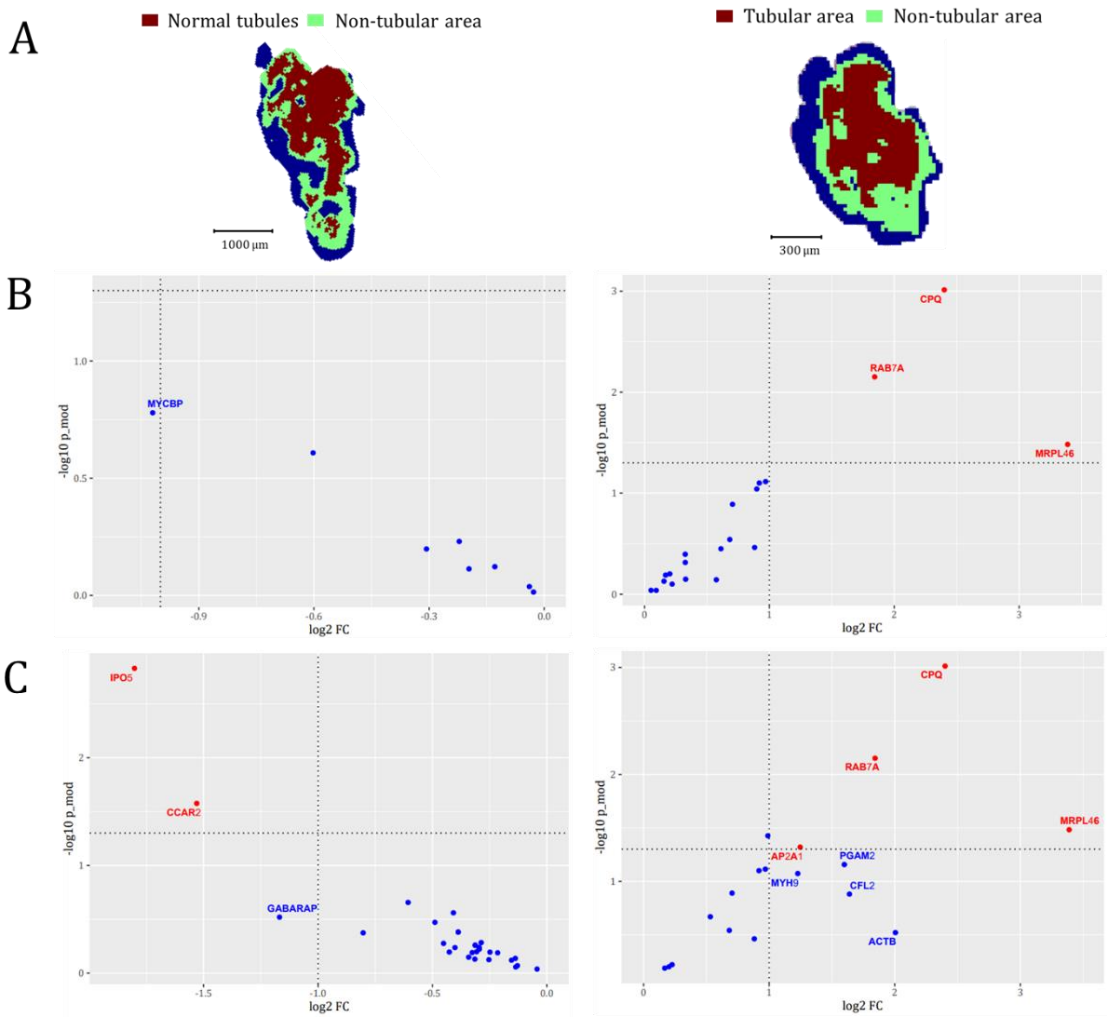

Figure 16. Protein identification *in situ* with the maximum likelihood for the MA2 testicular sample. (A) Segmentation map containing color-coded cluster legend that reflects morphological features of the tissue. (B) Part of Volcano plot that marks respective positions of the identified proteins (two-fold difference) detected in the brown cluster. (C) Same as (B) in respect to the lime cluster. Left side – proteins identified in fertile donor; right side - proteins identified in MA2 sample

3.3.4. Biological processes represented by *in situ* identified proteins from MA2

GO term analysis of identified processes in clusters from MA2 patient and respective control is summarized in Figure 17. Analysis of the MA2 tubular cluster revealed the presence of processes such as regulation of protein localization of adherens junction and regulation of protein localization to the cell-cell junction (Figure 17A), which are important for the maintenance of functional BTB (Kolasa et al., 2011). Other identified proteins, participating in the blood coagulation process, were significantly upregulated in LC-MS measurement of MA patient samples (Figure 11B). Furthermore, proteins identified in MA2 non-tubular cluster also mostly participated in junction assembly, organization and regulation (Figure 17B).

Detected processes in the tubular cluster of the PS sample were metabolic-related, comprising of aldonic acid catabolic and metabolic process and monosaccharide metabolic process among others (Figure 17C). In the interstitial cluster of the control sample, immune activity was detected in the form of neutrophil degranulation and activation (Figure 17D).

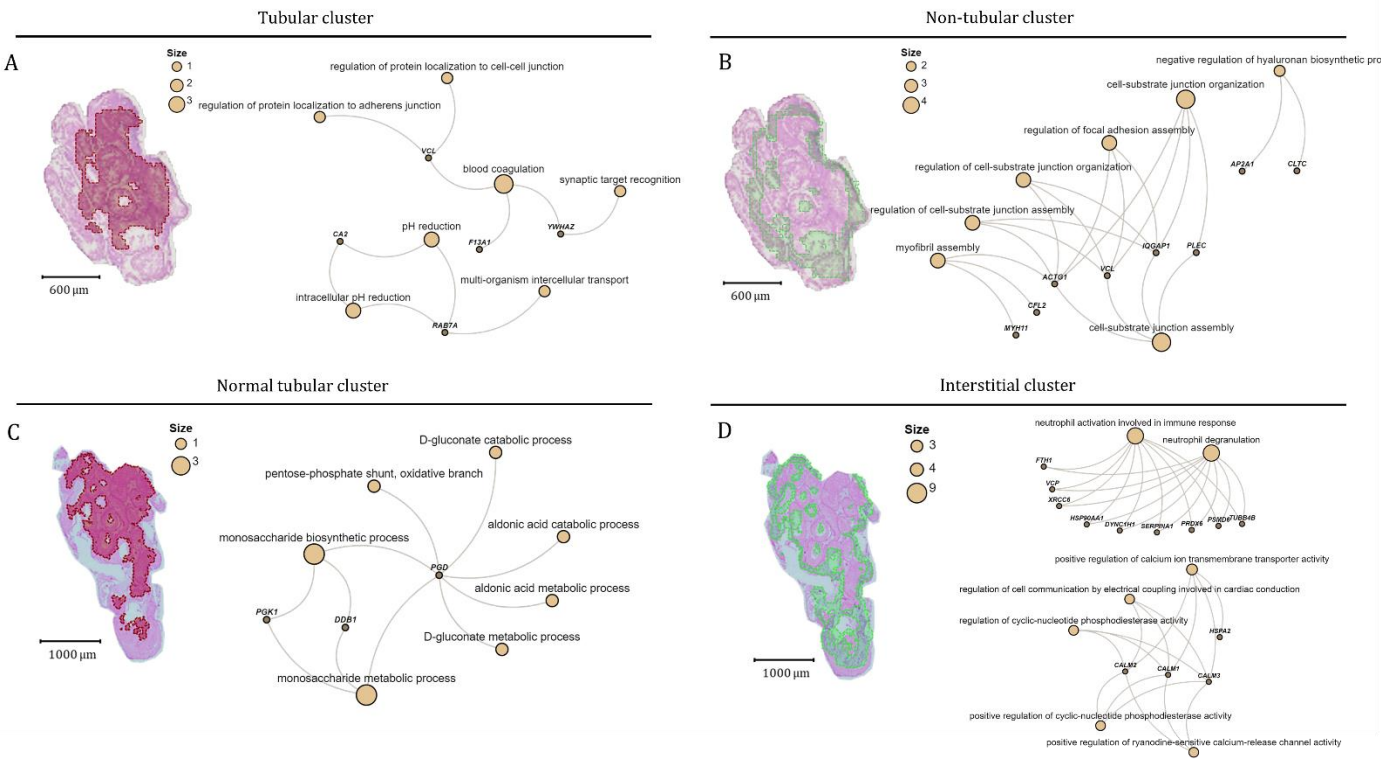

Figure 17. Gene ontology (GO) term analysis of proteins identified in each cluster of MA2 patient and control. The right side shows the overlay of segmentation map showing the cluster of interest and the H&E stained optical image of the sample, while the left side shows the go term analysis corresponding to the cluster. Results were obtained from (A) tubular cluster and (B) non-tubular cluster from MA patient 2, as well as (C) normal tubular cluster and (D) interstitial cluster from healthy fertile donor. The orange nodes indicate the biological processes, while the grey ones indicate the genes involved in each process. The size of the orange nodes (scale represented by numbered circle legend in the left corner) are representative of the number of genes involved in a particular biological process within the GO term map.

3.3.5. Protein identification *in situ* for SA1a testicular samples

Protein identification and GO term analysis were performed independently on both testicular biopsies from a patient with SA due to different morphological features. From the first biopsy, it was possible to identify proteins belonging to a cluster containing both tubular and interstitial areas and the one containing SCO tubules (Figure 18A). The software identified six enriched proteins in the first cluster combining main testicular compartments, seminiferous tubules and interstitium, out of which only ANHAK was not statistically

significant in the LC-MS analysis (Figure 18B, right). Identified proteins like PLEC, VIM and ANHAK have been associated with the structural support of the cell and the organization of cytoskeletal proteins at the plasma membrane (ElGhamrawy et al., 2014; Gentil et al., 2003; Guttman et al., 1999). Interestingly, in the SCO tubular cluster, 15 enriched proteins were identified, out of which 12 were statistically significant in the LC-MS analysis (Figure 18D, right). Since most of these proteins are involved in the pathophysiology of male infertility through their involvement in the regulation of blood coagulation, oxidative stress and inflammation (Heit et al., 2013; Paz et al., 2006; Siu et al., 2003), alongside their localization in defective tubules, they can serve as a potential source for protein biomarkers.

In the control samples, in both tubular (PGK2, LMAN2, LZIC, TOMM34) and interstitial areas (TXTL1, CCT4, HSPA2, CCT8), four statistically significant proteins were identified (Figure 18B-C, left).

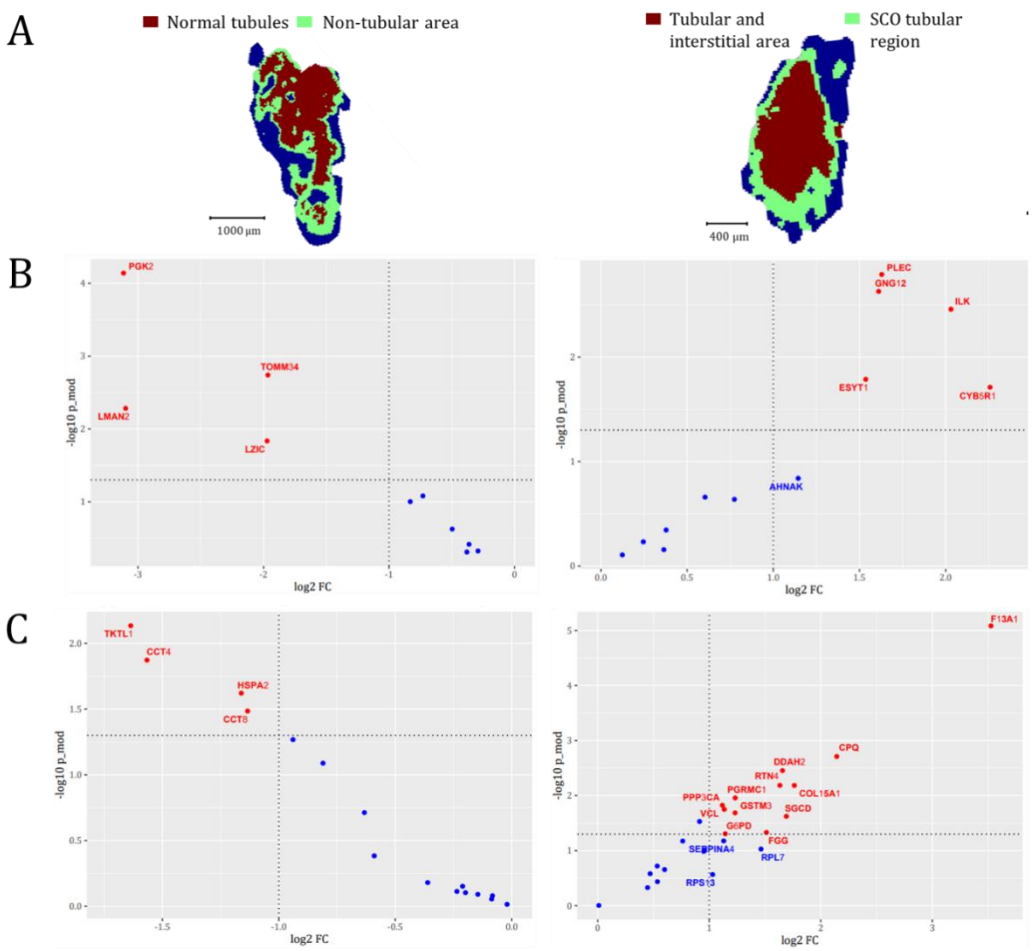

Figure 18. Protein identification *in situ* with the maximum likelihood for the SA1a testicular sample. (A) Segmentation map containing color-coded cluster legend that reflects morphological features of the tissue. (B) Part of Volcano plot that marks respective positions of the identified proteins (two-fold difference) detected in the brown cluster. (C) Same as (B) in respect to the lime cluster. Left side – proteins identified in fertile donor; right side - proteins identified in SA1a sample

3.3.6. Biological processes represented by *in situ* identified proteins from SA1a

GO term analysis of identified processes in clusters from the first biopsy of a patient diagnosed with SA and respective control is summarized in Figure 19. Analysis of SA1a tubular cluster revealed the presence of processes such as platelet degranulation, prenylcisteine catabolic and metabolic process, response to calcium and processes involved in vesicular transport (Figure 19A). However, proteins identified in SCO tubular cluster were

involved in striatal muscle cell differentiation and plasma membrane organization which are regulated by peritubular myoid cells. Those cell surround the seminiferous tubules in the testis and their impaired function was associated with azoospermia (Losinno et al., 2012) (Figure 19B).

In the control tissue, proteins identified in the normal tubular cluster were involved in catabolic and metabolic-related processes such as aldonic-acid and D-gluconate metabolic processes (Figure 19C). The interstitial cluster consisted of regulatory processes involved in cyclic-nucleotide phosphodiesterase activity and calcium ion transmembrane transporter activity (Figure 19D).

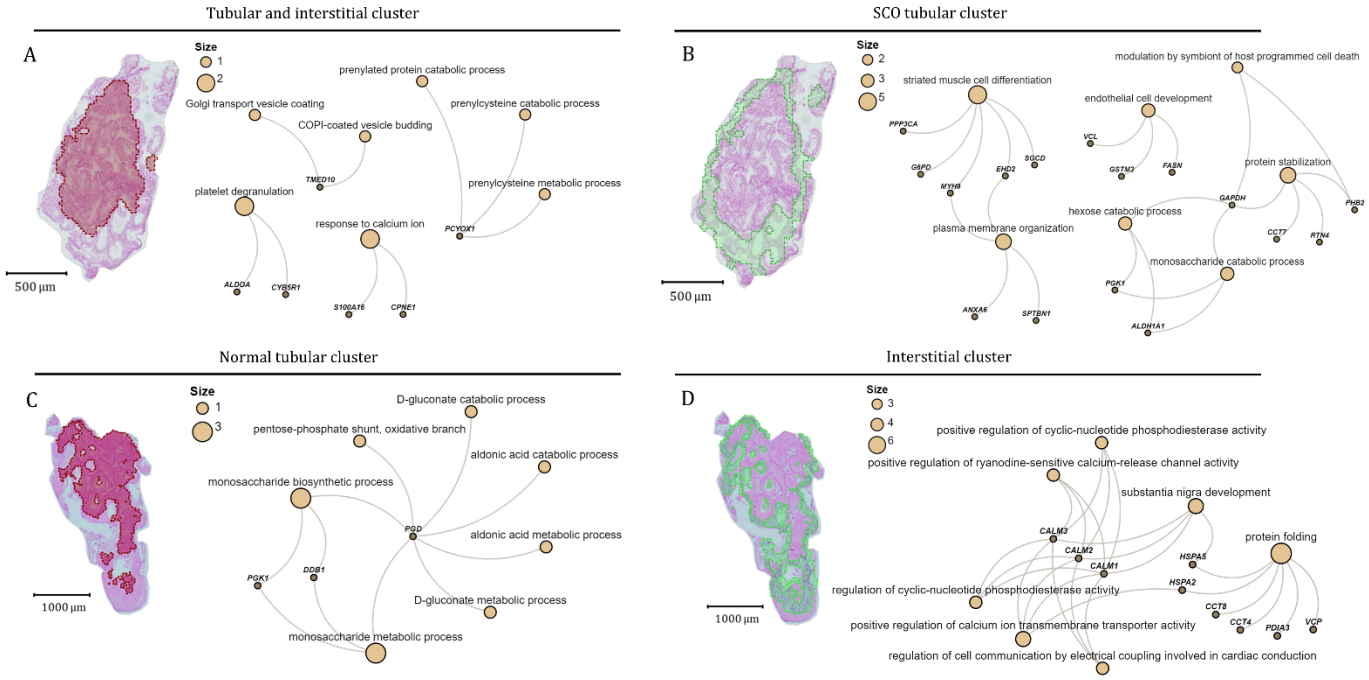

Figure 19. Gene ontology (GO) term analysis of proteins identified in each cluster of SA1a, and control. The right side shows the overlay of segmentation map showing the cluster of interest and the H&E stained optical image of the sample, while the left side shows the go term analysis corresponding to the cluster. Results were obtained from (A) tubular and interstitial cluster and (B) SCO tubular cluster from first biopsy of SA patient 1, as well as (C) normal tubular cluster and (D) interstitial cluster from healthy fertile donor. The orange nodes indicate the biological processes, while the grey ones indicate the genes involved in each process. The size of the orange nodes (scale represented by numbered circle legend in the left corner) are representative of the number of genes involved in a particular biological process within the GO term map.

3.3.7. Protein identification *in situ* for SA1b testicular samples

In the SA1b, clusters were histo-pathologically assigned to a tubular and non-tubular areas (Figure 20). In the tubular cluster, six enriched proteins were identified out of which PLEC and VIM contribute to the formation and regulation of cell structural support and cell-cell adhesion (Figure 20B, right) (ElGhamrawy et al., 2014). In addition, the PRDX3 gene previously detected in the tubular cluster of MA1 patient, is also detected in the tubular cluster of the SA1b. As mentioned above, it plays a critical role in the regulation of sperm function and male fertility (Ryu et al., 2017). In the non-tubular cluster, 11 enriched proteins were identified out of which eight were statistically significant (HLA-DRA, VIM, G6PD, PLEC, CA1, EZR, SRM, HMGCS2, TKT) in LC-MS analysis (Figure 20C, right).

Identified proteins present in the tubular area of control tissue were following: LMAN2, ACRBP and RPS4Y1 (Figure 20B, left). In the interstitial cluster of the control sample, five enriched proteins were identified (TKTL1, SOF2L1, HSP90AA1, GYG1, GABARAP) (Figure 20C, left).

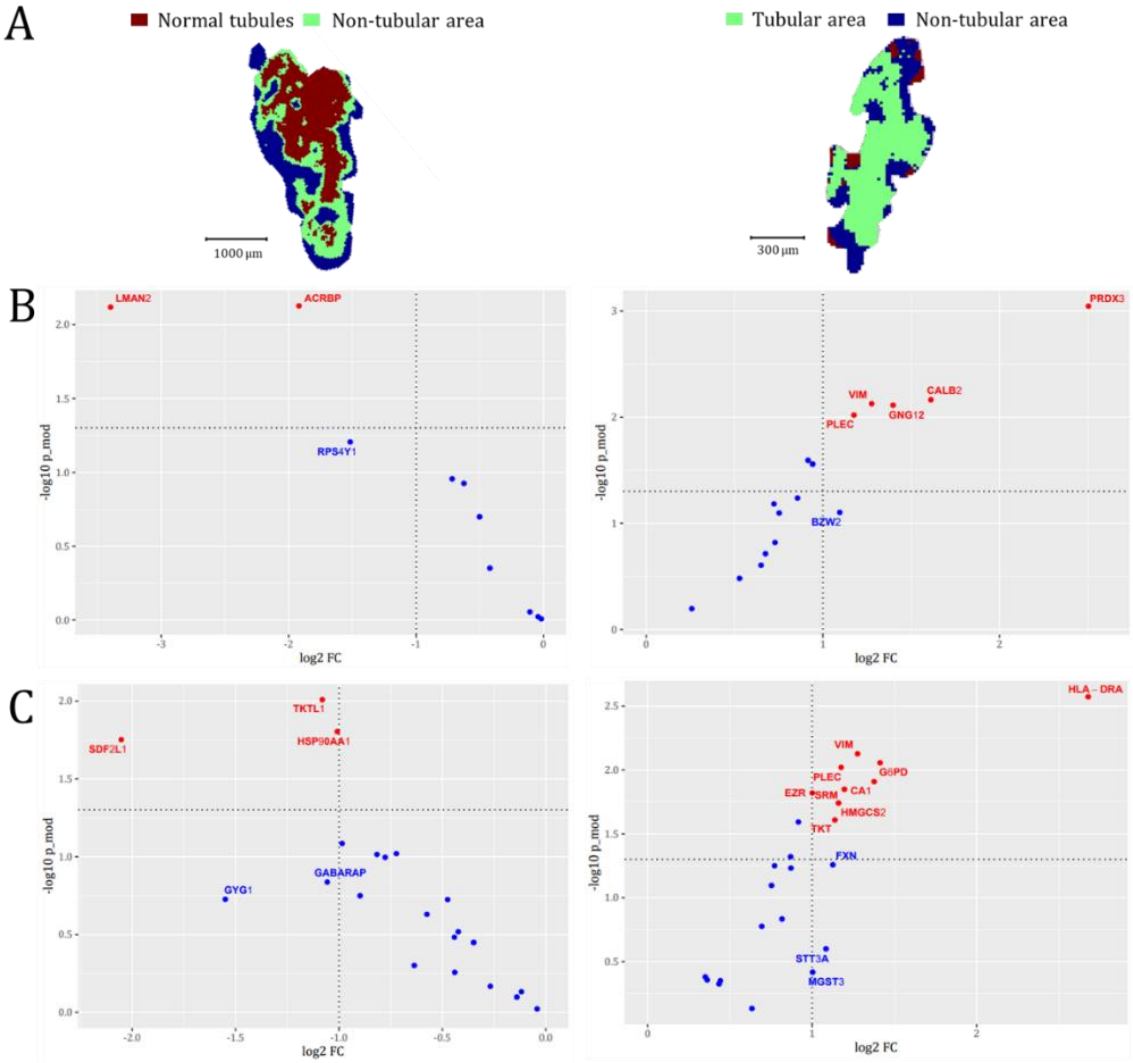

Figure 20. Protein identification *in situ* with the maximum likelihood for the SA1b testicular sample. (A) Segmentation map containing color-coded cluster legend that reflects morphological features of the tissue. (B) Part of Volcano plot that marks respective positions of the identified proteins (two-fold difference) detected in the brown cluster in case of control, and lime in case of SA1b. (C) Same as (B) in respect to the lime cluster (control) and deep-blue cluster (SA1b). Left side – proteins identified in fertile donor; right side - proteins identified in SA1b sample

3.3.8. Biological processes represented by *in situ* identified proteins from SA1b

The majority of the biological processes that were correlated with the proteins detected in the tubular cluster of the SA1b, were involved in DNA regulation-related processes involving DNA replication, double-strand break repair, centrosome complex assembly and so on (Figure 21A). In the non-tubular cluster, identified proteins were associated with regulation of muscle system process, epithelial cell-cell adhesion, cell-substrate junction assembly and pentose metabolic and biosynthetic process (Figure 21B).

In the control tissue, proteins identified in the normal tubular cluster were involved in the cellular response to fluoride and vitamin E, as well as in adenine transport and positive regulation of the Wnt signaling pathway (Figure 21C). However, in the interstitial cluster, biological processes like DNA replication and telomere capping and organization were detected (Figure 21D).

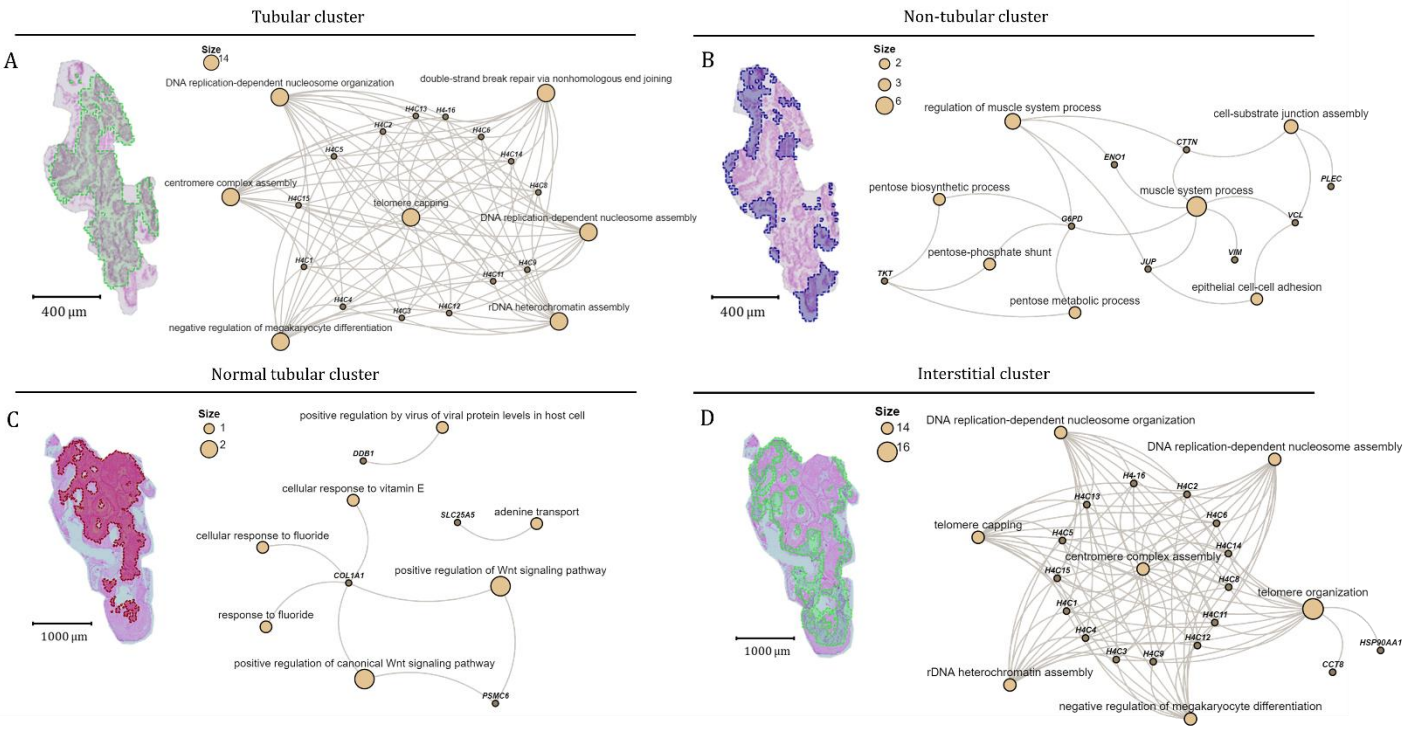

Figure 21. Gene ontology (GO) term analysis of proteins identified in each cluster of SA1b and control. The right side shows the overlay of segmentation map showing the cluster of interest and the H&E stained optical image of the sample, while the left side shows the go term analysis corresponding to the cluster. Results were obtained from (A) tubular cluster and (B) non-tubular cluster from second biopsy of SA patient 1, as well as (C) normal tubular cluster and (D) interstitial cluster from healthy fertile donor. The orange nodes indicate the biological processes, while the grey ones indicate the genes involved in each process. The size of the orange nodes (scale represented by numbered circle legend in the left corner) are representative of the number of genes involved in a particular biological process within the GO term map.

4. Discussion

4.1. Optimization and validation of a MALDI imaging protocol for FFPE tissues

MALDI IMS has evolved as a histology-based mass spectrometry technique that enables label-free multiplexed detection and analysis of molecules in their native histological state. In recent years, it gained increasing impact on scientific studies and diagnostics and has already been successfully used in biological and clinical research for analyses of multiple molecular species in their histological context from various tissue samples (Norris & Caprioli, 2013b).

Until recently, fresh frozen tissue samples were preferentially used in imaging mass spectrometry since FFPE samples were believed to be unusable (Schwamborn & Caprioli, 2010). Notably, FFPE tissue specimens provide valuable molecular information in tissue-based research, they are readily available in clinic and much easier to conserve than fresh frozen tissue samples (Flores Bueso et al., 2020; Ly et al., 2016). To date, reported approaches differ widely in process and efficacy. Additionally, optimized sample preparation protocol for MALDI IMS remains an essential requirement for each sample type since it is highly dependent on the complexity of the tissue sample and the physicochemical properties of the analytes of interest (Fowler et al., 2013; Judd et al., 2019).

Contrary to fresh frozen tissue, where proteins can be measured directly in their native intact form, FFPE samples do not offer the same possibility due to the formation of protein crosslinks during the formalin fixation step. Since these crosslinks make the proteins unavailable and inaccessible for desorption and detection, they are enzymatically digested into peptides that serve as surrogates for their precursor proteins (Judd et al., 2019; Maraschin et al., 2017; O'Rourke & Padula, 2016). Heat-based protein unfolding also known as the AR step, de-crosslinks the proteins and improves *in situ* digestion. Therefore, it is the most important protocol optimization step that is necessary to obtain a higher number of peptide signals. The efficiency of the AR method depends on the temperature, time, pH and chemical composition of the buffer. Furthermore, the best method that prevents morphological damage and allows proper epitope unmasking must be determined

empirically (BioGenex, 2020; Judd et al., 2019). For that reason, two methods were compared: OI and HP. Although HP microwave cooker is the most commonly used equipment, OI at lower temperature is used when working with fragile tissue sections as higher temperature may damage or distort tissue morphology. Our data confirmed that the choice of AR method has a significant impact on the resulting MALDI IMS data. The number of peptide peaks obtained in OI was two to four times higher than the one detected while using the HP method. Manzulli et al. (2021) regarded mass spectra with S/N ratios higher than 3 as high-quality spectra with relatively high S/N ratios that typically permit detection of 50 to 100 mass peaks per spectrum. Additionally, Mourino-Alvarez et al. (2016) obtained MALDI IMS results using fresh frozen tissue sections with 140 peptide signals detected with satisfactory intensities (S/N ratio >3). This protocol optimization led to the detection of more than 100 mass peaks with an average S/N ratio of around 20 indicating that the applied parameters generated spectra well above the quality threshold.

Since *in situ* peptide generation is the only way of observing proteins in FFPE tissues, solution conditions of the proteolytic enzyme trypsin, play a major role in determining the results. Two trypsin solutions that are commonly used in enzymatic digestion processes were compared (Judd et al. 2019, Ly et al. 2019). The main difference between the two conditions was the addition of 0.01% glycerol (Ly et al., 2016) that is commonly used for the ionization of membrane proteins. However, no significant differences were detected and therefore, the data was not shown. The solution composition proposed by Judd et al. (2019) led to the detection of a slightly higher overall peptide count with increased intensity and was therefore used in all further measurements. Following this, the *in situ* digestion temperature was optimized to retain the maximal yield of peptide signals while minimizing analyte delocalization. Two incubation temperatures were tested (37°C and 50°C). Although higher temperature ensured increased peptide signal detection, the 37°C incubation temperature retained the spatial-molecular features to a higher degree.

Next, we optimized the matrix deposition temperature using an HTX TM-Sprayer. Since increasing the temperature at which the matrix solvent is applied to the sample minimizes analyte delocalization (Veličković et al., 2020), three elevated temperatures were compared: 85°C, 70°C and 60°C. Using 85°C temperature resulted in a non-homogeneous matrix

deposition, most likely due to rapid solvent evaporation. This would lead to the formation of matrix crystals in the nozzle of the sprayer causing discontinuous matrix deposition. Homogeneous matrix deposition is of the utmost importance because it ensures that the detected pattern in an ion image is a reflection of molecular content and not the matrix deposition flaw or crystallization artifact. Detection of higher overall peptide number in combination with highly retained spatial-molecular features resulted in choosing 70°C deposition temperature over the 60°C for preparation of FFPE tissue samples.

Furthermore, validation of the optimized protocol for FFPE testicular tissues was carried out using human clinical samples. The successful translation of research from the mouse testis to human patient samples was evident by comparing the spectral properties and spatial distributions of peptides between the two datasets. Additionally, this confirmed the applicability of the method when using different sources of tissue material, since there were no observable differences between the datasets. Therefore, the protocol has proven to be reliable and reproducible, while ensuring a high molecular detection level.

4.2. Proteomic signatures of idiopathic testicular tissue

Despite technological advances, the cause of male infertility remains unknown in 60%–75% of cases classifying them as idiopathic (Jung & Seo, 2014; Wu et al., 2010). The main challenge faced in the field of male infertility is a lack of understanding of the underlying molecular mechanisms that affect the physiological function of spermatogenesis due to its complex biological system. Many studies have focused on determining the molecular pathways associated with male infertility using large-scale –omics techniques that allow a much deeper molecular understanding of the disease-related phenotype. Since genomics alone has proven to be insufficient for a full description of a biological system, proteomics has emerged as another large-scale platform for more accurate reflection of the dynamic state of a cell, tissue, or organism that will further improve the understanding of underlying biology (Amiri-Dashatan et al., 2018). Moreover, it has proven to be a promising tool for diagnostic and therapeutic biomarker discovery since it offers comprehensive information regarding the protein distribution, as well as molecular and functional pathways associated with the identified peptides (Agarwal et al., 2020; Panner Selvam & Agarwal, 2020). Thus far, most proteomic studies have focused on sperm and seminal fluid analysis (Panner Selvam & Agarwal, 2018), which reflect the end-point in the process of spermatogenesis. However, the testis is the primary organ that generate abnormalities leading to impaired reproductive function. It can therefore provide spatiotemporal information and ultimately a better understanding of the functional protein network in spermatogenesis (Cooke & Saunders, 2002; Liu et al., 2013; Macleod & Varmuza, 2013).

In this study, a comparative protein profiling of two subtypes of testicular failure, associated with non-obstructive azoospermia, was performed. MA, characterized with simultaneous occurrence of both functional and SCO tubules in variable proportions and SA, characterized by germ cell maturation arrest in certain differentiation stage were analyzed. They represent common phenotypic manifestations of male infertility, for which no sperm proteomic studies can be performed since azoospermia is associated with the absence of sperm in the ejaculate (Agarwal et al., 2020), making a testicular proteomic study evermore necessary. With the aim of determining the molecular basis of previously mentioned idiopathic conditions at the

protein level, two complementary strategies were used combining spatially resolving power of MALDI IMS with the high-resolution ability of shotgun proteomics. The study was performed using a small number of human testicular biopsies, making it a pilot study. For this extensive proteomic analysis of the testicular FFPE tissue, a previously established MALDI IMS protocol for fresh-frozen tissues was used (Lahiri et al., 2021), which allowed the successful detection, identification and analysis of testis proteome.

The differences between the control group (PS), MA, and especially SA patients reflected the different cellular composition of these testis samples. Furthermore, the difference observed within different patients of MA may show the cellular and pathological heterogeneity associated with different human subjects. Many differentially expressed proteins in MA and SA tissue from azoospermia patients provided invaluable information about molecular mechanisms regulating sperm production. The findings are consistent with the results from limited previous reports (Alikhani et al., 2017; Drabovich et al., 2013; Silber et al., 1997), and can assist us in understanding the molecular complexity of male infertility through target identification.

4.2.1. Shotgun proteomic profiling and comparison between two types of impaired spermatogenesis

Following initial LC-MS sample preparation optimization, about 2,000 quantifiable proteins were identified from each patient. Between the sample groups, low variation in the number of identified proteins demonstrated the robustness and high reproducibility of the implemented protocol.

Subsequent LC-MS/MS data analysis, using LIMMA moderated t-test, revealed a total of 1817 and 1776 different proteins in two experimental groups (MA and SA) in comparison to the fertile donor. Further statistical analysis of the identified proteins revealed 480 and 820 DEPs in the case of MA and SA, respectively. The relatively lower number of DEPs in the MA group reflects the fact that atrophied testes contain both normal and impaired seminiferous tubules and therefore, more proteins will be shared with the healthy donor than in the case of the SA. The GO term analysis of those DEPs showed that these two infertility phenotypes have a

similar pathological fingerprint. The data demonstrated that proteins related to blood coagulation, hemostasis and immune response constituted the majority of highly upregulated proteins in tissue from MA and SA patients. Since maintenance of immune tolerance is of crucial importance for the protection of autoimmunogenic spermatozoa from attack from the self-immune system, its dysregulation can cause severe tissue damage. Induced testicular inflammation, therefore, presents an important etiological factor contributing to male infertility. However, thus far, there is little documented evidence on immunological infertility in men (Naito et al., 2012). The presence of hemorrhage-related processes indicates possible sites of tissue damage in the form of the disrupted endothelial wall leading to vascular injury, bleeding and the need for activation of the coagulation process that could have been caused by the presence of unrestrictive innate immune response (Cheng & Mruk, 2012). Furthermore, both histopathological subtypes of the non-obstructive azoospermia show downregulation of protein translation and cell cycle progression processes such as G2/M transition process that are required for successful cell proliferation and differentiation. Detected exclusively in the diseased tissue of both infertility phenotypes were also neurotransmitter-related processes regulating its level, transport and activity. Although it is known that mammalian and invertebrate germ cells express receptors for various neurotransmitters and modulators and possess several neurotransmitter transporters that modulate essential sperm functions including fertilization, motility, respiration and chemotaxis, the role of neurotransmitters and their underlying molecular mechanisms remains unknown (Onaivi et al., 2005; Ramírez-Reveco et al., 2017). For instance, the SNCG gene, detected in both pathologies, is involved in the regulation of neurotransmitter levels and transportation, more specifically in dopamine secretion. In comparison with other neurotransmitters, dopamine is a highly reactive molecule whose intracellular accumulation causes sperm motility inhibition, while its degradation produces oxidative species such as hydrogen peroxide whose catabolic process was highly upregulated in MA testis tissue (Ramírez-Reveco et al., 2017).

On the other hand, the study also revealed pathways and proteins distinguishing MA from SA testicular tissue. In MA patients, the strong upregulation of linker histone H1 variants involved in the regulation of chromatin silencing was detected indicating the change in

chromatin remodeling that could alter normal germ cell differentiation (Carrell & Hammoud, 2009). Recent studies have confirmed that the gene expression level of certain linker histone H1 subtypes plays an important part in the process of spermatogenesis and that their dysregulation triggers the chromatin structure abnormality, hindering the cell maturation that leads to male infertility (Yan et al., 2003; Ye et al., 2017). In accordance to the previous studies, downregulation of spliceosome-related proteins was observed in the MA patients. The presence of dynamic spliceosome complex is essential for cell survival and spermatogenesis due to the marked increase of alternative splicing of testes specific factors needed for the series of events from mitosis, meiosis and spermiogenesis (Chuma et al., 2009; Wu et al., 2016; Ye et al., 2017). Therefore, spliceosome dysregulation impairs the differentiation of spermatogonia, abolishing the maturation of germ cells into sperm. Another process observed exclusively in MA tissue is cyclase-inhibiting G protein-coupled receptor signaling pathway that causes a decrease in the cAMP level. Since cAMP plays a central role in cell signaling during sperm differentiation and maturation, decreasing its level could lead to the infertile phenotype related to defects in sperm motility and capacitation (Buffone et al., 2014). Furthermore, a decrease in intracellular cAMP level has also been shown to decrease the activity of AMPK that is an important regulator of cellular energy status (Omar et al., 2009). Since AMPK is closely related to lactate production and lactate is the central energy metabolite used by germ cells, an alteration of its production might cause some forms of male infertility (Boussouar & Benahmed, 2004).

Few detected biological processes distinguished SA from the MA group. For example, processes involving positive regulation of telomerase RNA localization to the Cajal body and protein folding were downregulated in the case of SA. Since the Cajal body plays an important role in the biogenesis of various ribonucleoproteins that are involved in mRNA processing, assembly and function of telomerase, it is highly required for efficient and rapid cell proliferation. Additionally, according to Martins et al. (2019), low levels of the proteins that are involved in this pathway such as CCT1, CCT2, CCT3, CCT4, CCT5 and RUVBL2, are related to low cell proliferation and induced cell apoptosis. Furthermore, dysregulation of the protein folding process can lead to the accumulation of defective proteins and result in the impaired male infertility (Samanta et al., 2019). The proteins involved in spermatid development and

regulation of protein polymerization were one of the most affected biological processes in the SA group. It has been shown that the dysregulation of proteins contributing to spermatid development inevitably leads to halted self-renewal and differentiation of germ stem cell line and in that way interferes with late stages of spermatogenesis and fertilization. Additionally, proteins involved in the regulation of protein polymerization such as SPTB, CTNNA2, ARL2, ARFIP1, DMTN and DBN1 have been associated with actin filament assembly and organization. Since actin filament bundles are very abundant at the BTB, their disorganization has been associated with the disruption of its integrity and function (Cheng & Mruk, 2012; Yan et al., 2007). Additionally, defects of these genes result in the immobilization of the actin cytoskeleton and inhibition of the proper morphological changes in cells that lead to impaired spermatid development during spermiogenesis (Cheng & Mruk, 2010; Vogl et al., 2008; Yan et al., 2007).

4.2.2. Identification of proteins and associated biological processes in spatiotemporal context

To the best of our knowledge, this is the first integrative study combining MALDI IMS with LC-MS data to investigate various infertility conditions (MA and SA) while using clinical testicular samples.

This strategy allowed the identification and molecular characterization of distinctive sets of seminiferous tubules in the MA samples based on the differential regional expression of proteins. The first set of tubules, histologically annotated as atrophied tubules, was defined by peptides derived from a series of proteins involved in spermatogenesis and immune response-related processes. The dosage imbalance of those proteins, such as FABP3, was shown to lead to an imbalance between proliferation and apoptosis, and could therefore be implicated in impaired spermatogenesis (Oztekin et al., 2020; Shen et al., 2013). Interestingly, a high expression of another identified protein, CKB, was detected in spermatozoa of infertile men diagnosed with asthenozoospermia and oxidative stress (Park & Pang, 2021). This further suggests that the proposed histological annotation represents atrophied tubules. The second set of tubules annotated as the ones with intact spermatogenesis was characterized by proteins associated with metabolic processes. Cells within the testis that participate in

normal spermatogenesis usually have a high metabolic demand. Highly upregulated proteins such as CA2, ALDOC and PRDX identified in those tubules have been directly associated with functional sperm motility and viability as well as the maintenance of HCO_3^- and ROS homeostasis. Dysregulation of any of these genes has proven to cause oxidative stress, DNA fragmentation and apoptosis of spermatozoa alongside the substantial reduction in sperm mobility and viability that ultimately leads to male infertility (Ryu et al., 2017; Wandernoth et al., 2015; Zhang et al., 2021). The tubular cluster of PS was characterized by proteins associated with the regulation of mitochondrial function. Proteins such as HSP90AA1 and HSPA2 have previously been associated with sperm maturity and male fertility. Both are expressed by germ cells in the testicular tissue and have been proposed as biochemical markers of human sperm function. Furthermore, a decline in their expression has been correlated with meiosis failure, progressive loss of germ cells, increased apoptosis and male infertility (Grad et al., 2010; Naaby-Hansen et al., 2010)**.** The synchronous occurrence of tubules with intact spermatogenesis alongside the tubules with different extent of spermatogenic impairment in the same tissue biopsy (Agarwal et al., 2020), makes the MALDI IMS technique and the data integration workflow optimal for analyzing the MA tissue. These results highlighted the potential of this technique to successfully discriminate between those two sets of tubuli and identify the proteins and processes required for proper spermatogenesis.

With this approach, it was also possible to detect inter-patient variability between two patients diagnosed with MA. Those proteins and associated processes, detected exclusively in one but not the other patient, distinguish the patterns of different spermatogenic defects present in MA. In the MA2 patient tissue, in contrast to MA1, non-tubular and to a lesser extent tubular cluster were characterized by the proteins, such as VCL and PLEC, involved cell-junction assembly and organization. The presence and restructuring of cellular junctions at the Sertoli-Sertoli and Sertoli-germ cell interface is of crucial importance for the maintenance of BTB. Therefore any disruption of these proteins can lead to dysfunctional spermatogenesis (Lee et al., 2009).

Lastly, the method was able to distinguish between two subtypes of NOA– SA and MA. For the SA, two biopsies, belonging to the same patient, were analyzed containing clusters with

various annotations: a) cluster containing tubular and interstitial area, b) SCO cluster, c) tubular and d) non-tubular cluster. In the SA, proteins detected within SCO tubular cluster associated with biological processes like striated muscle cell differentiation and plasma membrane organization were not previously observed in either MA patient. These processes are regulated by peritubular myoid cells which surround the seminiferous tubules in the testis. They closely interact with Sertoli cells to support seminiferous tubule development and function (Rebourcet et al., 2014). Additionally, it has been postulated that they act synergistically to generate the basal lamina of the seminiferous tubule whose overproduction has previously been associated with SCO tubules (Tsai et al., 2012).

The implementation of this strategy enabled localized identification of proteins that defined particular *in situ* tissue compartments. Furthermore, it allowed the identification of substantially altered proteomic compositions of both seminiferous tubules and interstitial spaces between fertile donors and infertile patients pointing towards a severe impairment of spermatogenesis in both azoospermia subtypes. The ability of this combinatory approach to distinguish between various infertility conditions, and molecularly characterize inter-patient and inter-tubular heterogeneity, makes it a great platform for the identification of proteomic signatures in idiopathic cases of male infertility.

5. Conclusion

This study provided a strategy for performing *in situ* digestion and MALDI peptide imaging of FFPE testicular tissue specimens. This optimized strategy was successfully established by testing various parameters on mouse testicular biopsies to ensure high peptide yield while maintaining tissue integrity and preventing analyte delocalization and loss. Following initial optimization, its reliability and reproducibility were further tested on clinical samples giving rise to satisfactory results and enabling its further use in future FFPE research.

This pilot study aimed to provide an overall picture highlighting the proteomic signatures that could be implicated in idiopathic cases of male infertility. The proteomic data showed an altered proteomic profile in MA and SA compared with the fertile donor. These preliminary results have identified maturation failure, immune reaction response and hemostasis as the common causes for non-obstructive azoospermia. It was also demonstrated that translational machinery involving spliceosome proteins and linker histone variants was altered in the MA samples. Furthermore, proteins required for normal spermatogenesis and spermiation of the germ cells, involved in the regulation of actin assembly, were not detected in the SA group but were rather present exclusively in the control tissue.

Additionally, using an integrative analysis combining MALDI IMS with LC-MS, diverse spatiotemporal fingerprints of the identified proteins were visualized in the testicular tissue. Using this strategy, it was possible to distinguish different testicular compartments within the tissue section. Additionally, it was possible to successfully identify and molecularly characterize distinct sets of seminiferous tubules in the MA tissue, distinguishing between atrophied tubules and the ones with intact spermatogenesis. Furthermore, numerous proteins showed different regional expression in comparison to the fertile donor, when investigated by MALDI IMS, suggesting that they play an important role in the observed pathology. Therefore, this new integrative approach can provide a better insight into the complex pathological mechanisms of idiopathic male infertility. Furthermore, it could be broadly applicable in the precise pathological evaluation of target tissues in both preclinical and clinical settings and may become a high-throughput technique in biomarker discovery.

6. References

Agarwal, A., Hamada, A. & Esteves, S.C. 2015. Engaging practicing gynecologists in the management of infertile men. *J Obstet Gynaecol India,* 65(2):75-87.

Agarwal, A., Panner Selvam, M.K. & Baskaran, S. 2020. Proteomic Analyses of Human Sperm Cells: Understanding the Role of Proteins and Molecular Pathways Affecting Male Reproductive Health. *International journal of molecular sciences,* 21(5):1621.

Aichler, M. & Walch, A. 2015. MALDI Imaging mass spectrometry: current frontiers and perspectives in pathology research and practice. *Laboratory investigation,* 95(4):422-431.

Alexandrov, T. 2012. MALDI imaging mass spectrometry: statistical data analysis and current computational challenges. *BMC Bioinformatics,* 13 Suppl 16(Suppl 16):S11.

Alikhani, M., Mirzaei, M., Sabbaghian, M., Parsamatin, P., Karamzadeh, R., Adib, S., Sodeifi, N., Gilani, M.A.S., Zabet-Moghaddam, M., Parker, L., Wu, Y., Gupta, V., Haynes, P.A., Gourabi, H., Baharvand, H. & Salekdeh, G.H. 2017. Quantitative proteomic analysis of human testis reveals system-wide molecular and cellular pathways associated with non-obstructive azoospermia. *Journal of proteomics,* 162:141-154.

Amiri-Dashatan, N., Koushki, M., Abbaszadeh, H.-A., Rostami-Nejad, M. & Rezaei-Tavirani, M. 2018. Proteomics Applications in Health: Biomarker and Drug Discovery and Food Industry. *Iranian journal of pharmaceutical research : IJPR,* 17(4):1523-1536.

Angel, T.E., Aryal, U.K., Hengel, S.M., Baker, E.S., Kelly, R.T., Robinson, E.W. & Smith, R.D. 2012. Mass spectrometry-based proteomics: existing capabilities and future directions. *Chemical Society reviews,* 41(10):3912-3928.

Aziz, N. 2013. The importance of semen analysis in the context of azoospermia. *Clinics (Sao Paulo, Brazil),* 68 Suppl 1(Suppl 1):35-38.

BioGenex. 2020. *Microwave Antigen Retrieval Accessory Kit/ Pressure cooker* [Online] Available from: http://store.biogenex.com/download.php?filename=932-MW001.pdf (Accessed 15.07.2021)

BioRender. Available from: https://biorender.com/
(Accessed 13.06.2021)

Bonanomi, M., Lucente, G. & Silvestrini, B. 2002. Male fertility: core chemical structure in pharmacological research. *Contraception,* 65(4):317-320.

Boussouar, F. & Benahmed, M. 2004. Lactate and energy metabolism in male germ cells. *Trends Endocrinol Metab,* 15(7):345-350.

Bracke, A., Peeters, K., Punjabi, U., Hoogewijs, D. & Dewilde, S. 2018. A search for molecular mechanisms underlying male idiopathic infertility. *Reproductive BioMedicine Online,* 36(3):327-339.

Buffone, M.G., Wertheimer, E.V., Visconti, P.E. & Krapf, D. 2014. Central role of soluble adenylyl cyclase and cAMP in sperm physiology. *Biochimica et biophysica acta,* 1842(12 Pt B):2610-2620.

Carrell, D.T. & Hammoud, S.S. 2009. The human sperm epigenome and its potential role in embryonic development. *Molecular Human Reproduction,* 16(1):37-47.

Cassatella, D., Martino, N.A., Valentini, L., Guaricci, A.C., Cardone, M.F., Pizzi, F., Dell'Aquila, M.E. & Ventura, M. 2013. Male infertility and copy number variants (CNVs) in the dog: a two-pronged approach using Computer Assisted Sperm Analysis (CASA) and Fluorescent In Situ Hybridization (FISH). *BMC genomics,* 14(1):921.

Cheng, C.Y. & Mruk, D.D. 2010. A local autocrine axis in the testes that regulates spermatogenesis. *Nature Reviews Endocrinology,* 6(7):380-395.

Cheng, C.Y. & Mruk, D.D. 2012. The blood-testis barrier and its implications for male contraception. *Pharmacological reviews,* 64(1):16-64.

Chuma, S., Hosokawa, M., Tanaka, T. & Nakatsuji, N. 2009. Ultrastructural characterization of spermatogenesis and its evolutionary conservation in the germline: germinal granules in mammals. *Mol Cell Endocrinol,* 306(1-2):17-23.

Cioppi, F., Rosta, V. & Krausz, C. 2021. Genetics of Azoospermia. *International Journal of Molecular Sciences,* 22(6):3264.

Cocuzza, M., Alvarenga, C. & Pagani, R. 2013. The epidemiology and etiology of azoospermia. *Clinics (Sao Paulo, Brazil),* 68 Suppl 1(Suppl 1):15-26.

Cooke, H.J. & Saunders, P.T. 2002. Mouse models of male infertility. *Nat Rev Genet,* 3(10):790-801.

Cortés-Rodriguez, M., Royo, J.L., Reyes-Palomares, A., Lendínez, A.M., Ruiz-Galdón, M. & Reyes-Engel, A. 2018. Sperm count and motility are quantitatively affected by functional polymorphisms of HTR2A, MAOA and SLC18A. *Reprod Biomed Online,* 36(5):560-567.

Coscia, F., Doll, S., Bech, J.M., Schweizer, L., Mund, A., Lengyel, E., Lindebjerg, J., Madsen, G.I., Moreira, J.M. & Mann, M. 2020. A streamlined mass spectrometry–based proteomics workflow for large-scale FFPE tissue analysis. *The Journal of Pathology,* 251(1):100-112.

Cummins, J.M. & Jequier, A.M. 1994. Treating male infertility needs more clinical andrology, not less. *Hum Reprod,* 9(7):1214-1219.

Dada, R., Kumar, M., Jesudasan, R., Fernández, J.L., Gosálvez, J. & Agarwal, A. 2012. Epigenetics and its role in male infertility. *J Assist Reprod Genet,* 29(3):213-223.

De Kretser, D.M. & Baker, H.W. 1999. Infertility in men: recent advances and continuing controversies. *J Clin Endocrinol Metab,* 84(10):3443-3450.

de Macedo, C.S., Anderson, D.M. & Schey, K.L. 2017. MALDI (matrix assisted laser desorption ionization) Imaging Mass Spectrometry (IMS) of skin: Aspects of sample preparation. *Talanta,* 174:325-335.

Drabovich, A.P., Dimitromanolakis, A., Saraon, P., Soosaipillai, A., Batruch, I., Mullen, B., Jarvi, K. & Diamandis, E.P. 2013. Differential diagnosis of azoospermia with proteomic biomarkers ECM1 and TEX101 quantified in seminal plasma. *Sci Transl Med,* 5(212):212ra160.

El Ayed, M., Bonnel, D., Longuespée, R., Castellier, C., Franck, J., Vergara, D., Desmons, A., Tasiemski, A., Kenani, A. & Vinatier, D. 2010. MALDI imaging mass spectrometry in ovarian cancer for tracking, identifying, and validating biomarkers. *Medical science monitor: international medical journal of experimental and clinical research,* 16(8):BR233-245.

ElGhamrawy, T., Helmy, D. & Elall, H. 2014. Cadherin and vimentin immunoexpression in the testis of normal and induced infertility models of albino rats. *Folia morphologica,* 73(3):339-346.

Fisher, J.R. & Hammarberg, K. 2012. Psychological and social aspects of infertility in men: an overview of the evidence and implications for psychologically informed clinical care and future research. *Asian J Androl,* 14(1):121-129.

Flores Bueso, Y., Walker, S.P., Hogan, G., Claesson, M.J. & Tangney, M. 2020. Protoblock - A biological standard for formalin fixed samples. *Microbiome,* 8(1):122.

Fowler, C.B., O'Leary, T.J. & Mason, J.T. 2013. Toward improving the proteomic analysis of formalin-fixed, paraffin-embedded tissue. *Expert Review of Proteomics,* 10(4):389-400.

Fujimura, Y. & Miura, D. 2014. MALDI Mass Spectrometry Imaging for Visualizing In Situ Metabolism of Endogenous Metabolites and Dietary Phytochemicals. *Metabolites,* 4(2):319-346.

Gemoll, T., Roblick, U.J. & Habermann, J.K. 2011. MALDI mass spectrometry imaging in oncology. *Molecular Medicine Reports,* 4(6):1045-1051.

Gentil, B.J., Delphin, C., Benaud, C. & Baudier, J. 2003. Expression of the Giant Protein AHNAK (Desmoyokin) in Muscle and Lining Epithelial Cells. *Journal of Histochemistry & Cytochemistry,* 51(3):339-348.

Giusti, L., Angeloni, C. & Lucacchini, A. 2019. Update on proteomic studies of formalin-fixed paraffin-embedded tissues. *Expert Rev Proteomics,* 16(6):513-520.

Giusti, L. & Lucacchini, A. 2013. Proteomic studies of formalin-fixed paraffin-embedded tissues. *Expert Review of Proteomics,* 10(2):165-177.

Grad, I., Cederroth, C.R., Walicki, J., Grey, C., Barluenga, S., Winssinger, N., De Massy, B., Nef, S. & Picard, D. 2010. The molecular chaperone Hsp90α is required for meiotic progression of spermatocytes beyond pachytene in the mouse. *PloS one,* 5(12):e15770-e15770.

Greytak, S.R., Engel, K.B., Bass, B.P. & Moore, H.M. 2015. Accuracy of Molecular Data Generated with FFPE Biospecimens: Lessons from the Literature. *Cancer research,* 75(8):1541-1547.

Griswold, M.D. 2016. Spermatogenesis: The Commitment to Meiosis. *Physiol Rev,* 96(1):1-17.

Groseclose, M.R., Andersson, M., Hardesty, W.M. & Caprioli, R.M. 2007. Identification of proteins directly from tissue: in situ tryptic digestions coupled with imaging mass spectrometry. *Journal of Mass Spectrometry,* 42(2):254-262.

Guttman, J.A., Mulholland, D.J. & Vogl, A.W. 1999. Plectin is concentrated at intercellular junctions and at the nuclear surface in morphologically differentiated rat Sertoli cells. *The Anatomical Record,* 254(3):418-428.

Halder, A., Jain, M. & Kumar, P. 2015. Primary Testicular Failure: An Overview. *JBR JCDR,* 3:5.

Heit, C., Jackson, B.C., McAndrews, M., Wright, M.W., Thompson, D.C., Silverman, G.A., Nebert, D.W. & Vasiliou, V. 2013. Update of the human and mouse SERPIN gene superfamily. *Human genomics,* 7(1):22-22.

Hochstenbach, R. & Hackstein, J.H. 2000. The comparative genetics of human spermatogenesis: clues from flies and other model organisms. *Results Probl Cell Differ,* 28:271-298.

Hussein, M.R., Abou-Deif, E.S., Bedaiwy, M.A., Said, T.M., Mustafa, M.G., Nada, E., Ezat, A. & Agarwal, A. 2005. Phenotypic characterization of the immune and mast cell infiltrates in the human testis shows normal and abnormal spermatogenesis. Fertility and Sterility, 83(5):1447-1453.

Irie, M., Fujimura, Y., Yamato, M., Miura, D. & Wariishi, H. 2014. Integrated MALDI-MS imaging and LC–MS techniques for visualizing spatiotemporal metabolomic dynamics in a rat stroke model. *Metabolomics,* 10(3):473-483.

Jockusch, H., Holland, A., Staunton, L., Schmitt-John, T., Heimann, P., Dowling, P. & Ohlendieck, K. 2014. Pathoproteomics of testicular tissue deficient in the GARP component VPS54: the wobbler mouse model of globozoospermia. *Proteomics,* 14(7-8):839-852.

Judd, A.M., Gutierrez, D.B., Moore, J.L., Patterson, N.H., Yang, J., Romer, C.E., Norris, J.L. & Caprioli, R.M. 2019. A recommended and verified procedure for in situ tryptic digestion of formalin-fixed paraffin-embedded tissues for analysis by matrix-assisted laser

desorption/ionization imaging mass spectrometry. *Journal of Mass Spectrometry,* 54(8):716-727.

Jung, J.H. & Seo, J.T. 2014. Empirical medical therapy in idiopathic male infertility: Promise or panacea? *Clinical and experimental reproductive medicine,* 41(3):108-114.

Kokkat, T.J., Patel, M.S., McGarvey, D., LiVolsi, V.A. & Baloch, Z.W. 2013. Archived formalin-fixed paraffin-embedded (FFPE) blocks: A valuable underexploited resource for extraction of DNA, RNA, and protein. *Biopreservation and biobanking,* 11(2):101-106.

Kolasa, A., Marchlewicz, M., Wenda-Różewicka, L. & Wiszniewska, B. 2011. DHT deficiency perturbs the integrity of the rat seminiferous epithelium by disrupting tight and adherens junctions. *Folia histochemica et cytobiologica / Polish Academy of Sciences, Polish Histochemical and Cytochemical Society,* 49:62-71.

Krausz, C. & Riera-Escamilla, A. 2018. Genetics of male infertility. *Nat Rev Urol,* 15(6):369-384.

Lahiri, S., Aftab, W., Walenta, L., Strauss, L., Poutanen, M., Mayerhofer, A. & Imhof, A. 2021. MALDI-IMS combined with shotgun proteomics identify and localize new factors in male infertility. *Life Science Alliance,* 4:e202000672.

Lee, N.P.Y., Wong, E.W.P., Mruk, D.D. & Cheng, C.Y. 2009. Testicular cell junction: a novel target for male contraception. *Current medicinal chemistry,* 16(7):906-915.

Lenzi, A. 1995. Male infertility: Evaluation of human sperm function and its clinical application. *Journal of Endocrinological Investigation,* 18(6):468-488.

Levine, H., Jørgensen, N., Martino-Andrade, A., Mendiola, J., Weksler-Derri, D., Mindlis, I., Pinotti, R. & Swan, S.H. 2017. Temporal trends in sperm count: a systematic review and meta-regression analysis. *Hum Reprod Update,* 23(6):646-659.

Li, N., Wang, T. & Han, D. 2012. Structural, cellular and molecular aspects of immune privilege in the testis. *Frontiers in Immunology,* 3(152).

Lilford, R., Jones, A.M., Bishop, D.T., Thornton, J. & Mueller, R. 1994. Case-control study of whether subfertility in men is familial. *Bmj,* 309(6954):570-573.

Liu, M., Hu, Z., Qi, L., Wang, J., Zhou, T., Guo, Y., Zeng, Y., Zheng, B., Wu, Y., Zhang, P., Chen, X., Tu, W., Zhang, T., Zhou, Q., Jiang, M., Guo, X., Zhou, Z. & Sha, J. 2013. Scanning of novel cancer/testis proteins by human testis proteomic analysis. *Proteomics,* 13(7):1200-1210.

Longuespée, R., Fléron, M., Pottier, C., Quesada-Calvo, F., Meuwis, M.A., Baiwir, D., Smargiasso, N., Mazzucchelli, G., De Pauw-Gillet, M.C., Delvenne, P. & De Pauw, E. 2014. Tissue proteomics for the next decade? Towards a molecular dimension in histology. *Omics,* 18(9):539-552.

Losinno, A.D., Morales, A., Fernández, D. & Lopez, L.A. 2012. Peritubular Myoid Cells from Rat Seminiferous Tubules Contain Actin and Myosin Filaments Distributed in Two Independent Layers1. *Biology of Reproduction,* 86(5).

Ly, A., Buck, A., Balluff, B., Sun, N., Gorzolka, K., Feuchtinger, A., Janssen, K.-P., Kuppen, P.J.K., van de Velde, C.J.H., Weirich, G., Erlmeier, F., Langer, R., Aubele, M., Zitzelsberger, H., McDonnell, L., Aichler, M. & Walch, A. 2016. High-mass-resolution MALDI mass spectrometry imaging of metabolites from formalin-fixed paraffin-embedded tissue. *Nature Protocols,* 11(8):1428-1443.

Ly, A., Longuespée, R., Casadonte, R., Wandernoth, P., Schwamborn, K., Bollwein, C., Marsching, C., Kriegsmann, K., Hopf, C., Weichert, W., Kriegsmann, J., Schirmacher, P., Kriegsmann, M. & Deininger, S.-O. 2019. Site-to-Site Reproducibility and Spatial Resolution in MALDI–MSI of Peptides from Formalin-Fixed Paraffin-Embedded Samples. *PROTEOMICS – Clinical Applications,* 13(1):1800029.

Macleod, G. & Varmuza, S. 2013. The application of proteomic approaches to the study of mammalian spermatogenesis and sperm function. *Febs j,* 280(22):5635-5651.

Manzulli, V., Rondinone, V., Buchicchio, A., Serrecchia, L., Cipolletta, D., Fasanella, A., Parisi, A., Difato, L., Iatarola, M., Aceti, A., Poppa, E., Tolve, F., Pace, L., Petruzzi, F., Rovere, I.D., Raele, D.A., Del Sambro, L., Giangrossi, L. & Galante, D. 2021. Discrimination of Bacillus cereus Group Members by MALDI-TOF Mass Spectrometry. *Microorganisms,* 9(6):1202.

Maraschin, B.J., Silva, V.P.d., Rock, L., Sun, H., Visioli, F., Rados, P.V. & Rosin, M.P. 2017. Optimizing Fixation Protocols to Improve Molecular Analysis from FFPE Tissues. *Brazilian dental journal,* 28(1):82-84.

Martin-du Pan, R.C. & Campana, A. 1993. Physiopathology of spermatogenic arrest. *Fertility and Sterility,* 60(6):937-946.

Martins, A.D., Agarwal, A., Baskaran, S., Pushparaj, P.N., Ahmad, G. & Panner Selvam, M.K. 2020. Alterations of Spermatozoa Proteomic Profile in Men with Hodgkin's Disease Prior to Cancer Therapy. World J Mens Health, 38(4):521-534.

Mascarenhas, M.N., Flaxman, S.R., Boerma, T., Vanderpoel, S. & Stevens, G.A. 2012. National, regional, and global trends in infertility prevalence since 1990: a systematic analysis of 277 health surveys. *PLoS Med,* 9(12):e1001356.

Maymon, B.B.-S., Yogev, L., Paz, G., Kleiman, S.E., Schreiber, L., Botchan, A., Hauser, R. & Yavetz, H. 2002. Sertoli cell maturation in men with azoospermia of different etiologies. *Fertility and Sterility,* 77(5):904-909.

Meinhardt, A. & Hedger, M.P. 2011. Immunological, paracrine and endocrine aspects of testicular immune privilege. *Molecular and Cellular Endocrinology,* 335(1):60-68.

Mellor, A.L. & Munn, D.H. 2006. Immune privilege: a recurrent theme in immunoregulation? *Immunological Reviews,* 213(1):5-11.

Milewski, R., Milewska, A.J., Czerniecki, J., Leśniewska, M. & Wołczyński, S. 2013. [Analysis of the demographic profile of patients treated for infertility using assisted reproductive techniques in 2005-2010]. *Ginekol Pol,* 84(7):609-614.

Mittal, R.D. 2015. Tandem mass spectroscopy in diagnosis and clinical research. *Indian journal of clinical biochemistry : IJCB,* 30(2):121-123.

Mourino-Alvarez, L., Iloro, I., de la Cuesta, F., Azkargorta, M., Sastre-Oliva, T., Escobes, I., Lopez-Almodovar, L.F., Sanchez, P.L., Urreta, H., Fernandez-Aviles, F., Pinto, A., Padial, L.R., Akerström, F., Elortza, F. & Barderas, M.G. 2016. MALDI-Imaging Mass Spectrometry: a step forward in the anatomopathological characterization of stenotic aortic valve tissue. *Scientific Reports,* 6(1):27106.

Naaby-Hansen, S., Diekman, A., Shetty, J., Flickinger, C.J., Westbrook, A. & Herr, J.C. 2010. Identification of calcium-binding proteins associated with the human sperm plasma membrane. *Reproductive Biology and Endocrinology,* 8(1):1-12.

Naegelen, I., Beaume, N., Plançon, S., Schenten, V., Tschirhart, E.J. & Bréchard, S. 2015. Regulation of Neutrophil Degranulation and Cytokine Secretion: A Novel Model Approach Based on Linear Fitting. *Journal of immunology research,* 2015:817038-817038.

Naito, M., Terayama, H., Hirai, S., Qu, N., Lustig, L. & Itoh, M. 2012. Experimental autoimmune orchitis as a model of immunological male infertility. *Med Mol Morphol,* 45(4):185-189.

Nistal, M., Paniagua, R., Riestra, M.L., Reyes-Múgica, M. & Cajaiba, M.M. 2007. Bilateral prepubertal testicular biopsies predict significance of cryptorchidism-associated mixed testicular atrophy, and allow assessment of fertility. *Am J Surg Pathol,* 31(8):1269-1276.

Nordkap, L., Joensen, U.N., Blomberg Jensen, M. & Jørgensen, N. 2012. Regional differences and temporal trends in male reproductive health disorders: semen quality may be a sensitive marker of environmental exposures. *Mol Cell Endocrinol,* 355(2):221-230.

Norris, J.L. & Caprioli, R.M. 2013a. Analysis of tissue specimens by matrix-assisted laser desorption/ionization imaging mass spectrometry in biological and clinical research. *Chemical reviews,* 113(4):2309-2342.
Norris, J.L. & Caprioli, R.M. 2013b. Analysis of tissue specimens by matrix-assisted laser desorption/ionization imaging mass spectrometry in biological and clinical research. *Chem Rev,* 113(4):2309-2342.

O'Rourke, M.B. & Padula, M.P. 2016. Analysis of formalin-fixed, paraffin-embedded (FFPE) tissue via proteomic techniques and misconceptions of antigen retrieval. *Biotechniques,* 60(5):229-238.

Oatley, J.M. & Brinster, R.L. 2008. Regulation of spermatogonial stem cell self-renewal in mammals. *Annual review of cell and developmental biology,* 24:263-286.

Omar, B., Zmuda-Trzebiatowska, E., Manganiello, V., Göransson, O. & Degerman, E. 2009. Regulation of AMP-activated protein kinase by cAMP in adipocytes: roles for phosphodiesterases, protein kinase B, protein kinase A, Epac and lipolysis. *Cell Signal,* 21(5):760-766.

Onaivi, E.S., Sugiura, T. & Di Marzo, V. 2005. *Endocannabinoids: the brain and body's marijuana and beyond.* CRC Press.

Oztekin, E., Sevinc, R., Dursunoglu, D., Karadayı Akdam, N. & Korucu, N. 2020. How does seminal plasma fatty-acid binding protein-9 level change in infertile males? *Physiology international,* 107.

Panner Selvam, M.K. & Agarwal, A. 2017. Update on the proteomics of male infertility: A systematic review. *Arab journal of urology,* 16(1):103-112.

Panner Selvam, M.K. & Agarwal, A. 2018. A systematic review on sperm DNA fragmentation in male factor infertility: Laboratory assessment. *Arab J Urol,* 16(1):65-76.

Panner Selvam, M.K. & Agarwal, A. 2020. Sperm and Seminal Plasma Proteomics: Molecular Changes Associated with Varicocele-Mediated Male Infertility. *World J Mens Health,* 38(4):472-483.

Park, Y.-J. & Pang, M.-G. 2021. Mitochondrial Functionality in Male Fertility: From Spermatogenesis to Fertilization. *Antioxidants (Basel, Switzerland),* 10(1):98.

Paz, M., Morín, M. & Del Mazo, J. 2006. Proteome profile changes during mouse testis development. *Comp Biochem Physiol Part D Genomics Proteomics,* 1(4):404-415.

Petok, W.D. 2015. Infertility counseling (or the lack thereof) of the forgotten male partner. *Fertility and Sterility,* 104(2):260-266.

Poongothai, J., Gopenath, T.S. & Manonayaki, S. 2009. Genetics of human male infertility. *Singapore Med J,* 50(4):336-347.

Ramírez-Reveco, A., Villarroel-Espíndola, F., Rodríguez-Gil, J.E. & Concha, I.I. 2017. Neuronal signaling repertoire in the mammalian sperm functionality. *Biology of Reproduction,* 96(3):505-524.

Ravitsky, V. & Kimmins, S. 2019. The forgotten men: rising rates of male infertility urgently require new approaches for its prevention, diagnosis and treatment. *Biology of Reproduction,* 101(5):872-874.

Rebourcet, D., O'Shaughnessy, P.J., Pitetti, J.-L., Monteiro, A., O'Hara, L., Milne, L., Tsai, Y.T., Cruickshanks, L., Riethmacher, D., Guillou, F., Mitchell, R.T., van't Hof, R., Freeman, T.C., Nef, S. & Smith, L.B. 2014. Sertoli cells control peritubular myoid cell fate and support adult Leydig cell development in the prepubertal testis. *Development (Cambridge, England),* 141(10):2139-2149.

Ryu, D.-Y., Kim, K.-U., Kwon, W.-S., Rahman, M.S., Khatun, A. & Pang, M.-G. 2017. Peroxiredoxin activity is a major landmark of male fertility. *Scientific Reports,* 7(1):17174.

Samanta, L., Sharma, R., Cui, Z. & Agarwal, A. 2019. Proteomic analysis reveals dysregulated cell signaling in ejaculated spermatozoa from infertile men. *Asian Journal of Andrology,* 21(2):121-130.

Schwamborn, K. & Caprioli, R.M. 2010. MALDI Imaging Mass Spectrometry – Painting Molecular Pictures. *Molecular Oncology,* 4(6):529-538.

Selvaraju, V., Baskaran, S., Agarwal, A. & Henkel, R. 2020. Environmental contaminants and male infertility: Effects and mechanisms. *Andrologia*:e13646.

Shen, Y., Song, G., Liu, Y., Zhou, L., Liu, H., Kong, X., Sheng, Y., Cao, K. & Qian, L. 2013. Silencing of FABP3 inhibits proliferation and promotes apoptosis in embryonic carcinoma cells. *Cell Biochem Biophys,* 66(1):139-146.

Shi, S.R., Key, M.E. & Kalra, K.L. 1991. Antigen retrieval in formalin-fixed, paraffin-embedded tissues: an enhancement method for immunohistochemical staining based on microwave oven heating of tissue sections. *Journal of Histochemistry & Cytochemistry,* 39(6):741-748.

Silber, S.J., Nagy, Z., Devroey, P., Tournaye, H. & van Steirteghem, A.C. 1997. Distribution of spermatogenesis in the testicles of azoospermic men: the presence or absence of spermatids in the testes of men with germinal failure. *Human Reproduction,* 12(11):2422-2428.

Siu, M.K., Mruk, D.D., Lee, W.M. & Cheng, C.Y. 2003. Adhering junction dynamics in the testis are regulated by an interplay of beta 1-integrin and focal adhesion complex-associated proteins. *Endocrinology,* 144(5):2141-2163.

Song, S.H., Chiba, K., Ramasamy, R. & Lamb, D.J. 2016. Recent advances in the genetics of testicular failure. *Asian J Androl,* 18(3):350-355.

Steiner, C., Ducret, A., Tille, J.-C., Thomas, M., McKee, T.A., Rubbia-Brandt, L., Scherl, A., Lescuyer, P. & Cutler, P. 2014. Applications of mass spectrometry for quantitative protein analysis in formalin-fixed paraffin-embedded tissues. *PROTEOMICS,* 14(4-5):441-451.

Strohalm, M., Kavan, D., Novák, P., Volný, M. & Havlícek, V. 2010. mMass 3: a cross-platform software environment for precise analysis of mass spectrometric data. *Anal Chem,* 82(11):4648-4651.

Stuppia, L., Franzago, M., Ballerini, P., Gatta, V. & Antonucci, I. 2015. Epigenetics and male reproduction: the consequences of paternal lifestyle on fertility, embryo development, and children lifetime health. *Clin Epigenetics,* 7:120.

Sy, J. & Ang, L.C. 2019. Microtomy: Cutting Formalin-Fixed, Paraffin-Embedded Sections. *Methods Mol Biol,* 1897:269-278.

Tanca, A., Pagnozzi, D. & Addis, M.F. 2012. Setting proteins free: progresses and achievements in proteomics of formalin-fixed, paraffin-embedded tissues. *Proteomics Clin Appl,* 6(1-2):7-21.

Tsai, M.C., Cheng, Y.S., Lin, T.Y., Yang, W.H. & Lin, Y.M. 2012. Clinical characteristics and reproductive outcomes in infertile men with testicular early and late maturation arrest. *Urology,* 80(4):826-832.

van Vliet, E. 2014. Omics and Related Recent Technologies. In: Wexler, P. (ed.). *Encyclopedia of Toxicology (Third Edition)*. Oxford: Academic Press.

Veličković, D., Zhang, G., Bezbradica, D., Bhattacharjee, A., Paša-Tolić, L., Sharma, K., Alexandrov, T., Anderton, C.R. & Consortium, K. 2020. Response Surface Methodology As a New Approach for Finding Optimal MALDI Matrix Spraying Parameters for Mass Spectrometry Imaging. *Journal of the American Society for Mass Spectrometry,* 31(3):508-516.

Vogl, A., Vaid, K., Guttman, J. & Cheng, C. 2008. Molecular mechanisms in spermatogenesis. *Springer*.

Wandernoth, P.M., Mannowetz, N., Szczyrba, J., Grannemann, L., Wolf, A., Becker, H.M., Sly, W.S. & Wennemuth, G. 2015. Normal Fertility Requires the Expression of Carbonic Anhydrases II and IV in Sperm. *The Journal of biological chemistry,* 290(49):29202-29216.
Wenke, J.L., Rose, K.L., Spraggins, J.M. & Schey, K.L. 2015. MALDI Imaging Mass Spectrometry Spatially Maps Age-Related Deamidation and Truncation of Human Lens Aquaporin-0. *Invest Ophthalmol Vis Sci,* 56(12):7398-7405.

Wu, H., Sun, L., Wen, Y., Liu, Y., Yu, J., Mao, F., Wang, Y., Tong, C., Guo, X., Hu, Z., Sha, J., Liu, M. & Xia, L. 2016. Major spliceosome defects cause male infertility and are associated with nonobstructive azoospermia in humans. *Proceedings of the National Academy of Sciences,* 113(15):4134-4139.

Wu, W., Shen, O., Qin, Y., Niu, X., Lu, C., Xia, Y., Song, L., Wang, S. & Wang, X. 2010. Idiopathic male infertility is strongly associated with aberrant promoter methylation of methylenetetrahydrofolate reductase (MTHFR). *PloS one,* 5(11):e13884-e13884.

Xiao, S. & Xia, L. 2016. Quantity versus quality: the sperm war. *Asian J Androl,* 18(6):900-901.

Yan, H.H., Mruk, D.D., Lee, W.M. & Cheng, C.Y. 2007. Ectoplasmic specialization: a friend or a foe of spermatogenesis? *Bioessays,* 29(1):36-48.

Yan, W., Ma, L., Burns, K.H. & Matzuk, M.M. 2003. HILS1 is a spermatid-specific linker histone H1-like protein implicated in chromatin remodeling during mammalian spermiogenesis. *Proceedings of the National Academy of Sciences,* 100(18):10546-10551.

Yates III, J.R. 1998. Mass spectrometry and the age of the proteome. *Journal of Mass Spectrometry,* 33(1):1-19.

Ye, X., Feng, C., Gao, T., Mu, G., Zhu, W. & Yang, Y. 2017. Linker Histone in Diseases. *International journal of biological sciences,* 13(8):1008-1018.

Zhang, P.-f., Huang, Y.-l., Fu, Q., He, W.-t., Xiao, K. & Zhang, M. 2021. Integrated analysis of phosphoproteome and ubiquitylome in epididymal sperm of buffalo (Bubalus bubalis). *Molecular Reproduction and Development,* 88(1):15-33.

Zhang, Y., Fonslow, B.R., Shan, B., Baek, M.-C. & Yates, J.R., 3rd 2013. Protein analysis by shotgun/bottom-up proteomics. *Chemical reviews,* 113(4):2343-2394.

Zhao, S., Zhu, W., Xue, S. & Han, D. 2014. Testicular defense systems: immune privilege and innate immunity. *Cellular & molecular immunology,* 11(5):428-437.

Zubair, F., Laibinis, P.E., Swisher, W.G., Yang, J., Spraggins, J.M., Norris, J.L. & Caprioli, R.M. 2016. Trypsin and MALDI matrix pre-coated targets simplify sample preparation for mapping proteomic distributions within biological tissues by imaging mass spectrometry. *J Mass Spectrom,* 51(12):1168-1179.

7. Curriculum vitae

I was born in 1996 in Rijeka, Croatia. After finishing high school at First Croatian Gymnasium in Sušak in Rijeka, I enrolled in undergraduate studies in Molecular biology (2015), and in graduate studies in Molecular biology (2018), at the Faculty of Science, University of Zagreb. During my studies, I was involved in various student activities and research projects. I have participated in various internships in: Laboratory for Evolutionary Genetics (Dr. Tomislav Domazet Lošo) at Ruđer Bošković Institute; Laboratory for Trophic Interactions (Dr. Lucija Šerić Jelaska) and Laboratory for Plant Physiology (Ass. Prof. Dr. Željka Vidaković Cifrek) at Faculty of Science, University of Zagreb; Laboratory for Developmental Neuropathology (Prof. Dr. Goran Šimić) at Croatian Institute for Brain Research. Additionally, I did two international summer internships in the field of neuroscience including: Laboratory for Neurogenetics (Prof. Dr. Björn Brembs) at the Institute of Zoology, University of Regensburg, Germany (2018) and Laboratory for Neurodegenerative Diseases (Dr. Ioannis Sotiropoulos) at the Life and Health Sciences Research Institute, University of Mihno, Portugal (2019). Since the beginning of 2020 I am a working as a research assistant in Laboratory for Mass Spectrometry (Prof. Dr. Axel Imhof), at the Biomedical Center Munich, Ludwig Maximilian University, Germany where I also did my master's thesis research.

Moreover, I was a demonstrator for two years (2017-18) at Zoology and Plant Physiology courses for molecular biology students. I was a member of the Biology Students Association (BIUS) and eSTUDENT organization in the science popularization sector. I also volunteered in many science popularization events such as: Night of Biology, Scientific Picnic, Science Fair, Scientific Quart, Hour of Code and Day for Science.

I participated in several conferences: Keeping Your Brain Healthy 2018 and TEDx University of Zagreb: The Extraordinary Now 2018 (as a member of the organizing committee) , Zagreb Student congress of neuroscience 'Neuri' 2019, Rijeka (oral presentation: "Neuronal differentiation in developing and adult brain"), Students' Symposium in Biology and Life Sciences 2019, Zagreb (oral presentation: "The effect of mechanical stress on model plant *Arabidopsis thaliana* (L.) Heynh"; and as a member of the organizing committee), SymBioSE 2019, Glasgow (poster presentation: "Predation on the winter moth *Operophtera brumata* by carabid beetles, centipedes and spiders") and SymBioSE 2020, Groningen (oral presentation: "Stem cell therapy for the central nervous system: real possibility or false hope?"). I have written one review article for Gyrus (Croatian neuroscience journal run and published by students): "Viruses that affect the human brain" that has been accepted for publication. I received the Rector's Award for academic year 2018./2019. For the research "The effect of mechanical stress on model plant *Arabidopsis thaliana* (L.) Heynh". I was awarded the City of Rijeka Scholarship for excellence from 2015 to 2020 for academic achievements.